2.1 Introduction

Metallometogens, a metal containing liquid crystals, the properties of various metallic coordinating complexes can be combined with the physical properties of liquid crystals**.** Metallomesogens have been extensively studied due to their unique geometric structure and the ability to combine the optical, electronic and magnetic properties of transition metal complexes with liquid crystal ligands [1-5]. The forces of the Vander wall are responsible for the retention of molecules in the anisotrope phase of the liquid crystal in organic molecules. The greatest potential for intermolecular interactions to include weak metal-metal and metal-ligand effects can be opened by the incorporation of metal ions in liquid crystal molecules [5].

Vorlander reported the first metallomesogens in 1910 and found that alkali metal carboxylate, $R(CH_2)_nCOO\ Na$ has the conventional laminar flow characteristics of soap [6]. Vorlander reported the first organic transition metallomesogens based on diarylmercury with the smectic phase [7] **(Figure 1).**

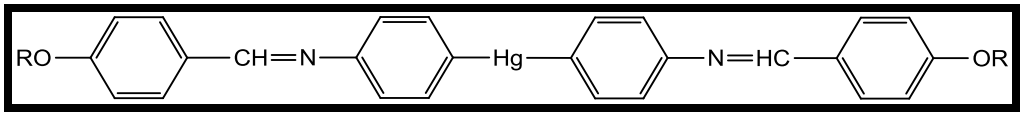

Figure 1. Organic transition metallomesogens based on diarylmercury

Heteroatoms contain organic molecules that can be bound to metals and can be used as ligands to form diverse coordination complexes with different metals, deepening their denticity. Salicylaldimine derivatives are widely used as ligands because of their potential for multiple substitution, their easy preparation, and their ability to coordinate with a wide variety of metals [8, 9]. Due to the presence of intramolecular hydrogen bonds between

hydroxyl and imine groups, liquid crystals based on salicylaldimine have thermal stability [10]. Transition metal complexes obtained from salicylaldimines are the most widely known complexes that exhibited mesogenic properties in metallo-mesogens. Nearly all 3d transition metal complexes derived from salicylaldimines show mesomorphic properties [11-19].

Mesomorphic behaviour of benzoxazoles-salicylaldimine derivatives with various transition metal ions like; Ni^{II}, Co^{II}, Cu^{II}, Pd^{II}, Zn^{II} studied by C.-J. Chen et al. [8] **(Figure 2).** They found that all Schiff bases ligands have N or/and SmC phases. They demonstrated the influence of metal ion geometry on the formation of mesophase complexes. Metallic ions coordinated by square planar geometry like Cu^{II}, Ni^{II} and Pd^{II} give phases N or/and SmC. The metal complexes of ZnII and CoII with tetrahedral geometry have no intermediate phase.

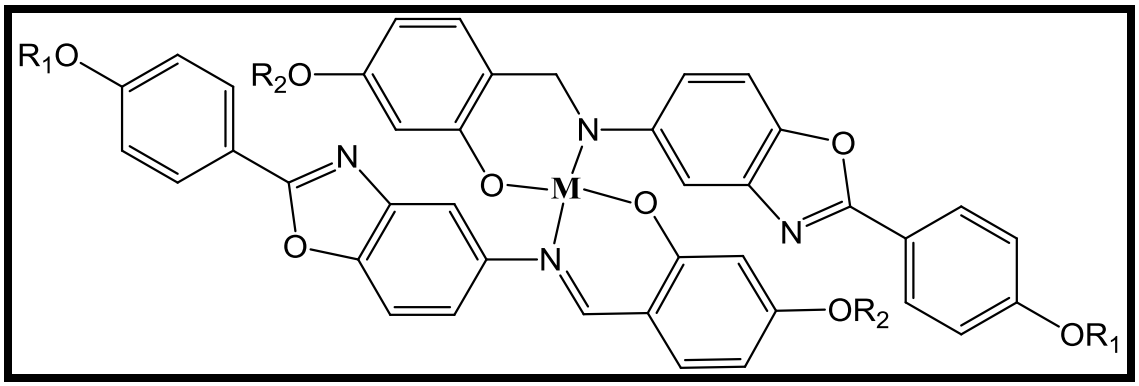

Figure 2. Metallomesogens of benzoxazoles-salicylaldimine derivatives

B.-T. Heng et al. [10] reported 1,2,3-triazole-based bidentate salicylaldimine and their analogues with terminal substituent (F, Cl, Br and I) with different length of terminal alkyl chain and their Cu(II) complexes **(Figure3).** All halogenated ligands and their Cu(II) complexes exhibited enantiotropic mesophase. They also found that fluorine-substituted complexes have the lowest phase transition temperature relative to chlorine, bromine and iodine-substituted complexes.

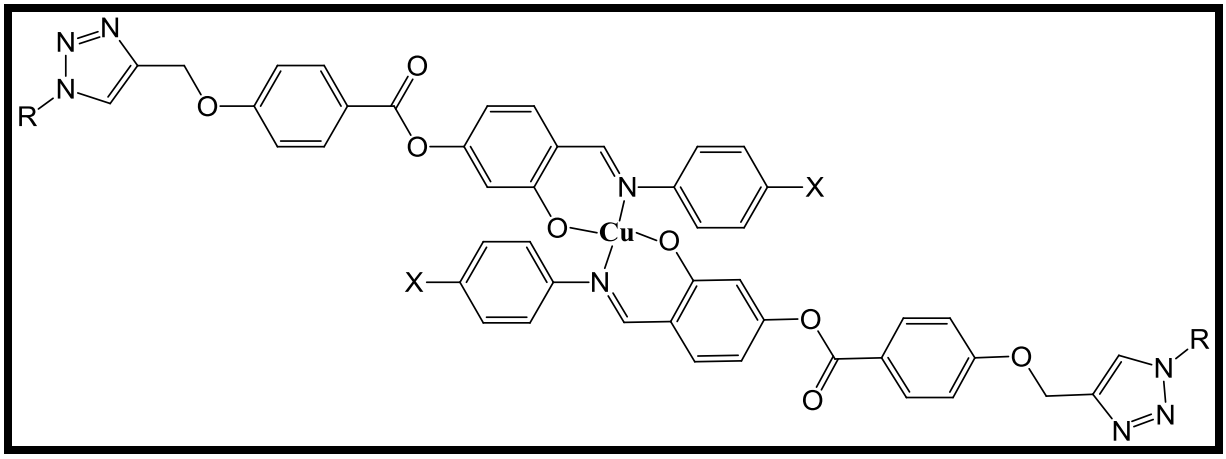

Figure 3. 1,2,3-triazole-based bidentate salicylaldimine and their Cu(II) complexes

A homologues series of bis[5-((4-alkoxyphenyl)azo)-N-(2-propanol) salicylal diminato] copper(II) complex were synthesized and their mesogenic behaviors studied by Z. Rezvani et al. [11] **(Figure 4).** Metallic copper complexes with *n*-tetradecyloxy and *n*-hexadecyloxy groups show a monotropic smectic-A, while *n*-decyloxy derivatives are not mesogenic. The researchers found that the *n*-hexadecyloxy derivatives have a larger mesogenic temperature range than the *n*-tetradecyloxy derivatives.

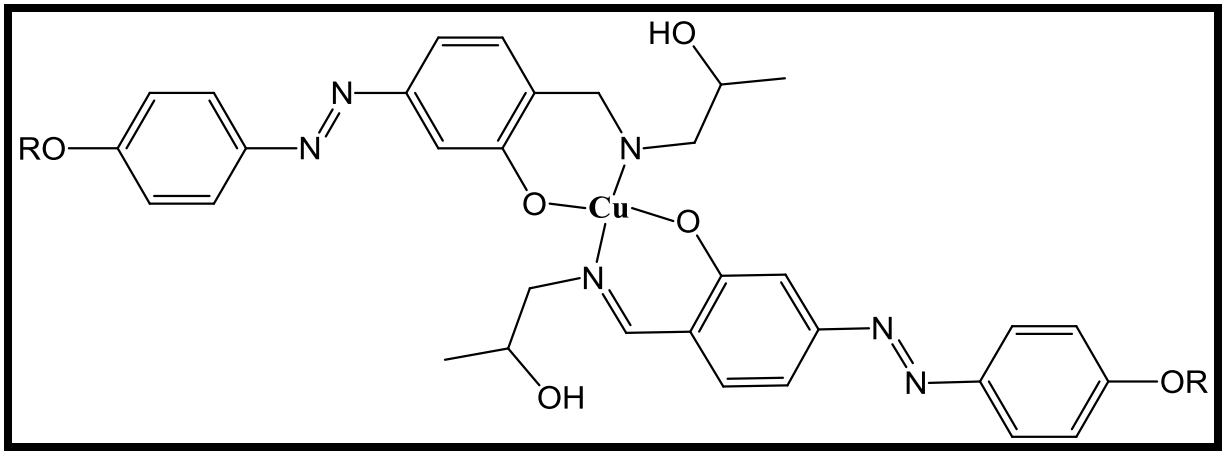

Figure 4. Bis[5-((4-alkoxyphenyl)azo)-N-(2-propanol) salicylaldiminato] copper(II) complex

K. Nejati et al. [12] reported *n*-decyloxy and *n*-dodecyloxy derivaties of 1,2-phenylene based salicylaldimine dimer, N,N'-di-(5-(4-alkoxyphenyl)azo)-salicylidene-1,2-phenylenediimine and their copper(II) complexes **(Figure 5).** Through the mesogenic study, they found that the ligands are not mesogenic, but the copper complexes of these ligands show the smectic-C mesophase with a narrow temperature range.

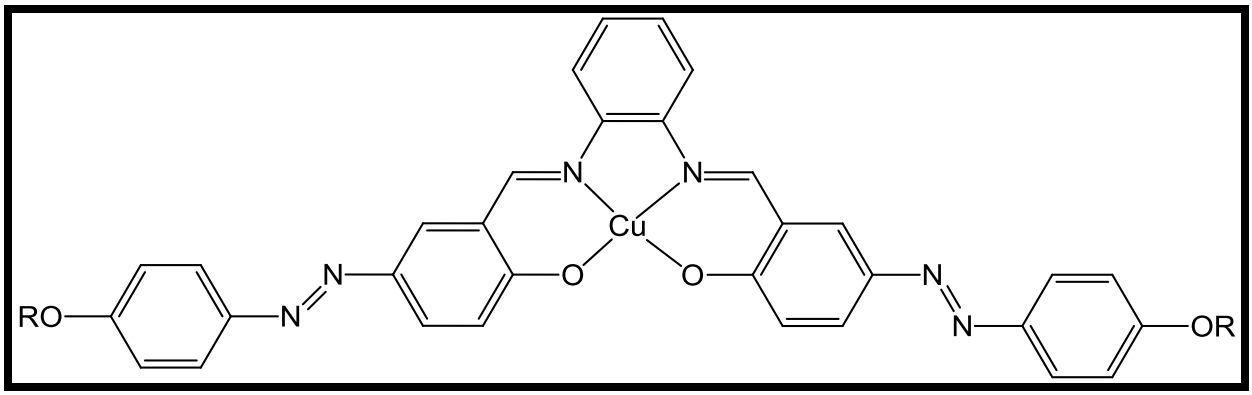

Figure 5. N,N'-di-(5-(4-alkoxyphenyl)azo)-salicylidene-1,2-phenylenediimine and their copper(II)

B. Singh et al. [13] have synthesized homologous series of N-(4-*n*-alkoxy-2-hydroxybenzylidene)-4-carbethoxyaniline with different alkoxy chain lengths (n = 6, 8, 10, 12, 16) and their Cu(II) metal complexes **(Figure6).** The mesomorphic study of this compound revealed that all the members of the series exhibited enantiotropic Sm-A phase with super cooling effect. The copper (II) complexes of the series also produced an enantiotropic SmA phase at higher temperatures, but the comparison with the ligands showed a narrower temperature range.

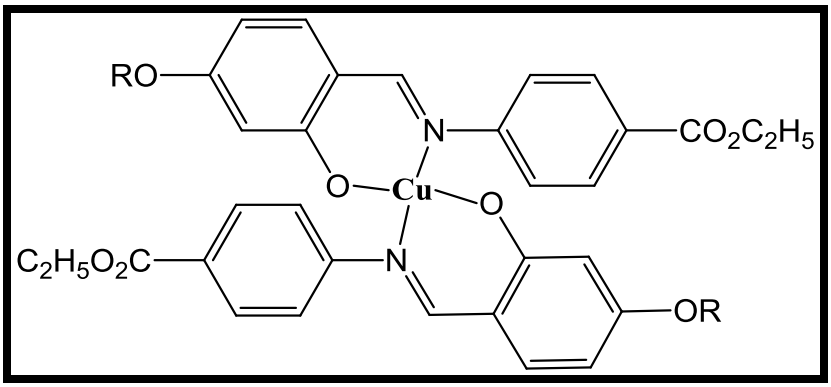

Figure 6. N-(4-*n*-alkoxy-2-hydroxybenzylidene)-4-carbethoxyaniline and their Cu(II) metal complexes

R. W. Date and D. W. Bruce [14] reported discotic salicylaldimato metal complexes of Ni, Pd, Cu and Fe–Cl with varying in chain length (n= 1, 4, 10, 16) and studied their liquid crystalline properties **(Figure 7).** They concluded that none of the ligands are mesogenic. All nickel complexes do not display mesophases. For all complexes containing *n*-methyl and *n*-butyl chains, no mesophases were observed. However, for both the *n*-decyl chain and the *n*-hexadecyl chain of the Pd and Fe-Cl complexes, have columnar mesophase.

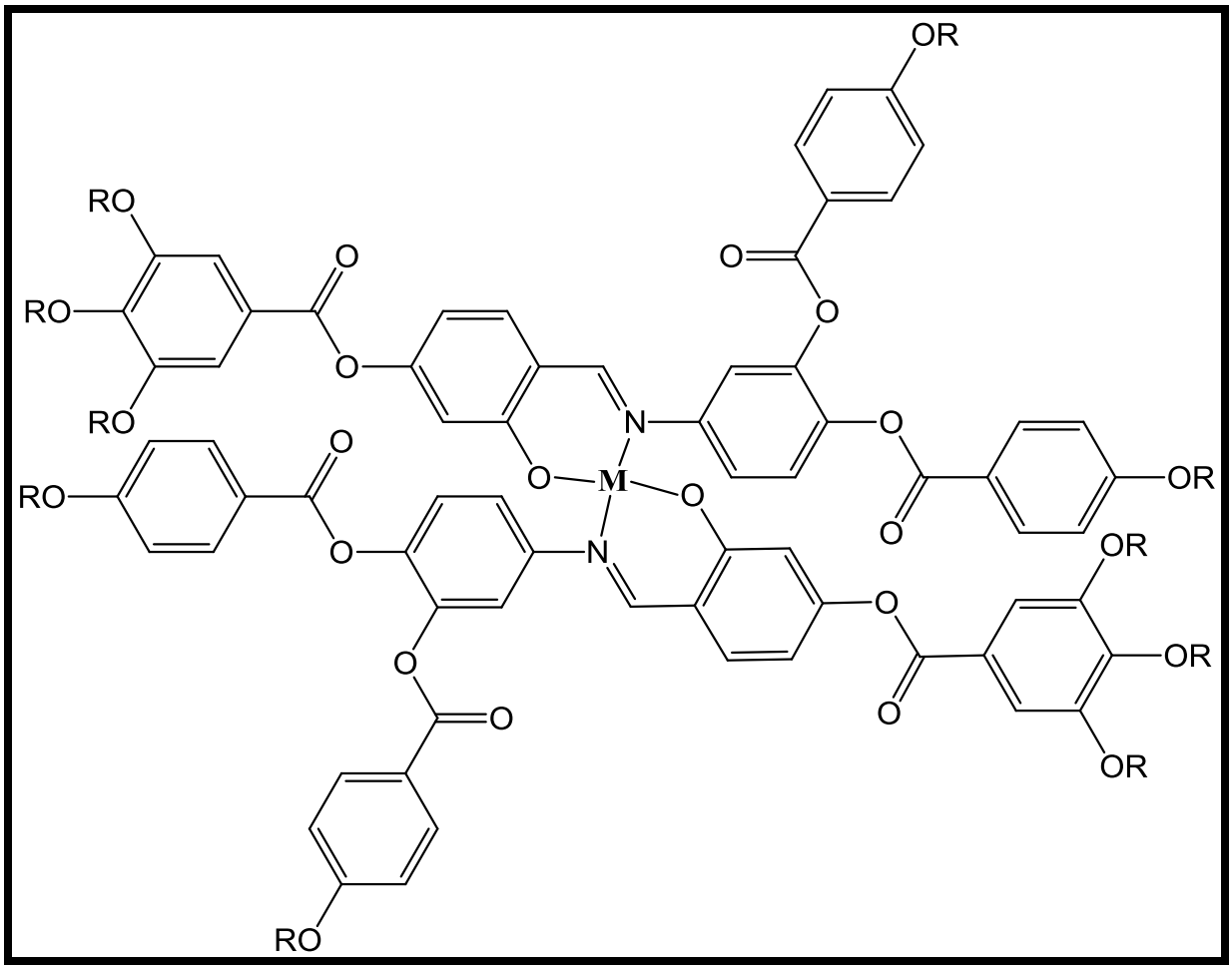

Figure 7. Discotic salicylaldimato metal complexes

Chung K. Lai and Yi-Fun Leu [15] have prepared bimetallomesogens complexes of copper (II), palladium(II), vanadyl(IV) and iron(III) chloride with salicylaldimine derivatives **(Figure 8).** Copper and palladium complexes are shown smectic A phase, but the complexes of vanadyl and ferric chloride are not mesogenic. They concluded that the geometric structure of the metal core contained in the tested complexes with oxygen bridges has a great influence on the liquid crystal properties.

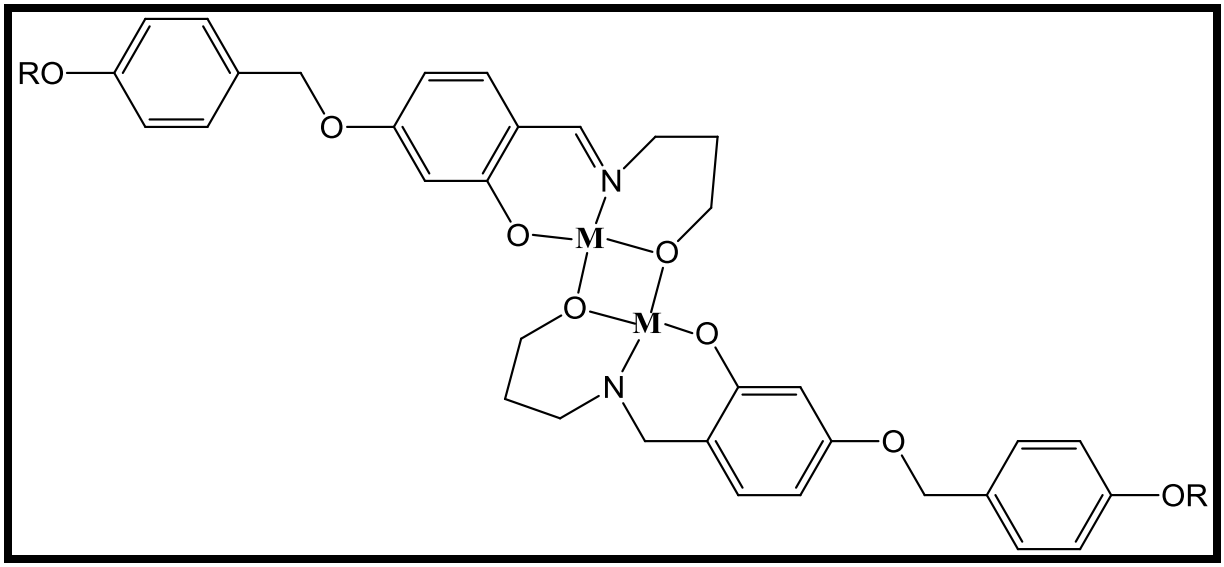

Figure 8. Bimetallomesogens complexes with different metal ions

In order to understand the effect of fine tuning of the 'salphen' ligand on the mesomorphic and photoluminescence behavior of the corresponding complexes, C.R. Bhattacharjee et al. [16] have synthesized a new series of mesogenic Zn(II)- salphen complexes with a chloro-substituted phenylnediamine spacer (**Figure 9**). The ligands of this series are not mesogenic or fluorescent. However, through the incorporation of Zn(II) metal ions, columnar rectangular mesophases (Colr) and fluorescent properties were observed.

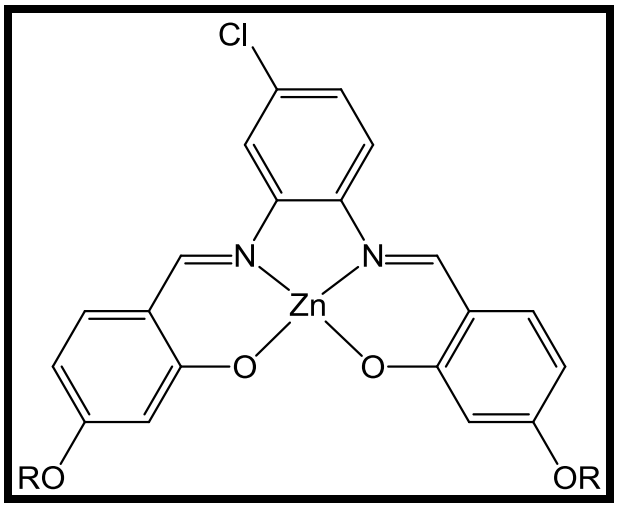

Figure 9. Zn(II)- salphen complexes

To understand the effect of the ligand structure on the mesomorphic behavior of lanthanide-containing salicylaldimine mesogens R. Van Deun and K. Binnemans [18] have synthesized lanthanide complexes with different, but structurally related Schiff 's base ligands **(Figure 10).** They observed that 4-substituted ligand with an increasing alkoxy chain length there as an increase in mesophase stability. If the alkoxy chain is not present, it becomes non-mesogenic. When alkoxy chain place changed from 4-position to 5-position, the corresponding metal complexes are non-mesogenic.

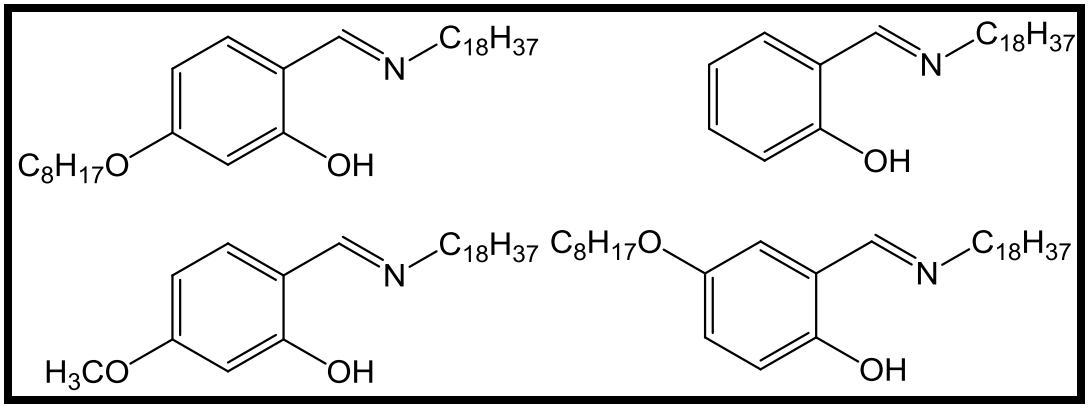

Figure 10. Structurally related Schiff base ligands

A. K. Prajapati and N. Bonde [19] have reported naphthyl-containing homologous series of mesogenic ligands and their Cu(II) complexes to understand the effect of the naphthalene moiety on mesomorphism **(Figure 11).** The series of ligands is purely nematogenic, whereas the incorporation of a Cu metal center into the ligand molecule leads to high thermal stability and formation of more ordered smectic-A mesophases. When compared with other structurally similar series, they conclude that the presence of the naphthalene moiety slightly reduces the thermal stability of the mesophase.

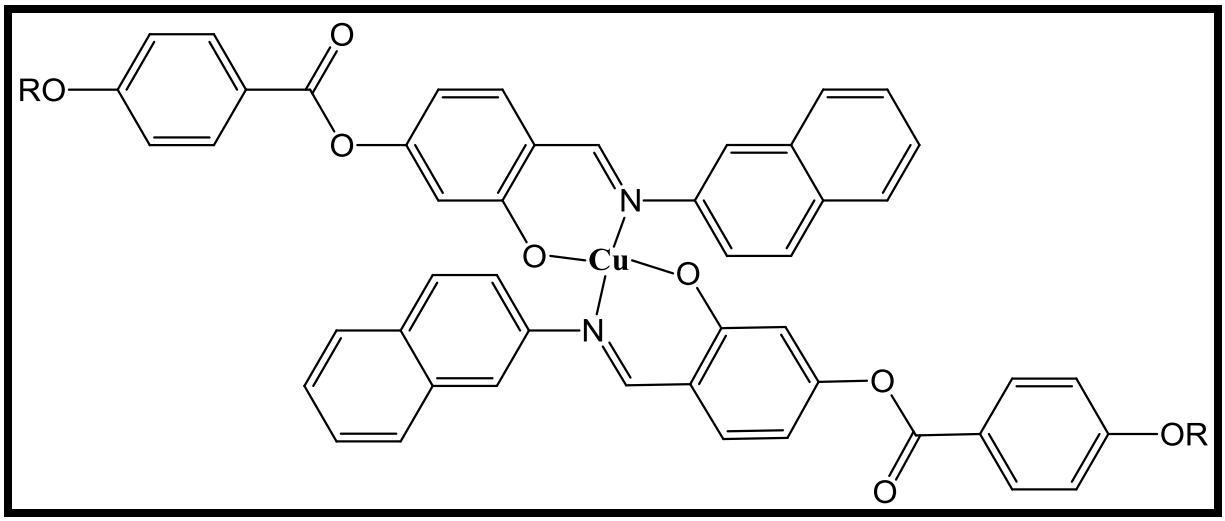

Figure 11. Naphthyl-containing mesogenic ligands and their Cu(II) complexes

In this work, we present the synthesis and liquid crystalline property of the new homologous series of the Schiff base of 4-*n*-alkoxy-2-hydroxybenzaldehyde with 4-amino acetophenone and their Cu(II) complexes.

2. 2 Experimental

2.2.1 Material

All reagents were procured from commercial sources and used as received. 2,4 dihydroxybenzaldehyde from TCI; alkyl bromides from SRL and Spectrochem; 4-aminoacetophenone from Lobachem. Copper(II) acetate hydrate from Spectrochem. Column chromatography separations were carried out with silica gel (60-120 mesh). The purity of the synthesized compounds was checked by using Silica Gel TLC Plate from Merck.

2.2.2 Characterization

The ^{1}H NMR spectra and ^{13}C NMR spectra were recorded on an AV 400 MHz Bruker FT-NMR spectrometer in $CDCl_3$ solution with tetramethylsilane(TMS) as an internal standard. IR spectra were recorded on Bruker spectrometer as KBr pellets. The mass spectrum was recorded on Water acquity Ultra performance LC with SQ detector. TG-DTA measurements were carried out on a SII EXSTAR6000TG-DTA instrument. The experiments were performed in N_2 at a heating rate of 10 ^{o}C min^{-1} in the temperature range 30-550 ^{o}C using an aluminum pan. Transition temperatures and enthalpies have been studied by DSC using a PerkinElmer thermal analyser with a heating and cooling rate of 10 ^{o}C min^{-1}. The Leica DM 2500P polarizing optical microscope provided with a Linkam heating stage was used to study the thermal behavior and optical texture of various compounds. Electronic spectra of the compounds in DMF were recorded on an Agilent UV Cary 60 spectrophotometer using a quartz cuvette. The Conduct metric measurements were carried out on EQUIP-TRONIC digital conductometer.

2.3 Synthesis

2.3.1 Synthesis of Series-A

2.3.1.1 Synthesis of 2-Hydroxy-4(*n*-alkoxy)benzaldehyde

2-Hydroxy-4(*n*-alkoxy)benzaldehyde were prepared by the following reported method [20].

2,4-Dihydroxybenzaldehyde (10 mmol, 1.38 g), $KHCO_3$ (10 mmol, 1 g), KI (catalytic amount) and the corresponding 1-bromoalkane (n=2 to 8, 10, 12, 14, 16, 18, 10 mmol) was mixed with 250 ml anhydrous acetone, refluxed for 24 h, then filtered hot to remove insoluble solids, neutralized the warm solution with dilute hydrochloric acid and extracted with chloroform (100 ml). Chloroform extract has been concentrated to obtain a violet solid. The solid was purified by column chromatography, using a mixture of ethyl acetate and petroleum ether (10% v/v) as eluent. Evaporating the solvent results in a yellow liquid (n = 2-8, 10) and a white solid (n = 12, 14, 16, 18) **(Scheme 1)**.

2-Hydroxy-4-(*n*-octyloxy)benzaldehyde.

Yellowish liquid; Yield 55%.^{1}H NMR (400 MHz ,$CDCl_3$,TMS) δ_H11.50 (s, ArO**H**, 1H), 9.71 (s, ArC**H**O, 1H), 7.42 (d, Ar**H**, 2H, *J* =8.8 Hz), 6.55-6.52 (dd, Ar**H**, 1H, *J* =8.8 Hz), 6.41 (d, Ar**H**, 1H, *J* =2.0 Hz), 4.01 (t, -OC**H$_2$**-, 2H), 2.06-1.25 (m, -O-C-(C**H$_2$**)$_6$-,12H), 0.91-0.87 (t, -C**H$_3$**, 3H); ^{13}CNMR (400MHz, $CDCl_3$, TMS) δ_C 194.3, 166.4, 164.5, 135.2, 114.9, 108.8, 101.0, 68.6, 31.8, 29.3, 29.2, 28.9, 25.9, 22.6,14.1; IR (υ_{max},cm^{-1},KBr : 3270 (υOH), 2954, 2856 (υ aliphatic C-H), 1727 (υC=O aldehyde), 1630 (υC=O ketone), 1575, 1507 (υ aromatic C=C), 1189, 1169 (υ PhO), 1116 (υ aliphatic C-O).

2-Hydroxy-4-(*n*-tetradecyloxy)benzaldehyde

White solid ; Yield: 62%; ^{1}H NMR (400 MHz, $CDCl_3$, TMS) δ_H 11.51 (s, ArO**H**, 1H), 9.72 (s, ArCO**H**, 1H), 7.43 (d, Ar**H**, 2H, *J*=8.8 Hz), 6.54 (dd, Ar**H**, 1H, *J*=8.8 Hz), 6.43 (d, Ar**H**, 1H, *J*=2.4 Hz), 4.03-4.00 (t, -OC**H$_2$**CH_2-, 2H), 1.88-1.27 (m, -C**H$_2$**-, 24H), 0.91-0.88 (t, -CH_2C**H$_3$**, 3H) ; IR (υ_{max}, cm^{-1}, KBr) : 3439 (υOH), 2912, 2849, (υ aliphatic C-H), 1728 (υC=O aldehyde), 1576, 1505 (υ aromatic C=C), 1187 (υ PhO), 1115 (υ aliphatic C-O).

2-Hydroxy-4-(*n*-hexadecyloxy)benzaldehyde

White solid ; Yield: 65%; ^{1}H NMR (400 MHz, $CDCl_3$, TMS) δ_H 11.51 (s, ArO**H**, 1H), 9.72 (s, ArCO**H**, 1H), 7.43 (d, Ar**H**, 2H, *J*=8.4 Hz), 6.54 (dd, Ar**H**, 1H, *J*=8.8 Hz), 6.43 (d, Ar**H**, 1H, *J*=2.4 Hz), 4.03-4.00 (t, -OC**H$_2$**CH_2-, 2H), 1.84-1.27 (m, -C**H$_2$**-, 28 H), 0.91-0.88 (t, -CH_2C**H$_3$**, 3H). IR (υ_{max}, cm^{-1}, KBr): 3437 (υOH), 2923, 2843, (υ aliphatic C-H), 1695 (υC=O aldehyde), 1578, 1509 (υ aromatic C=C), 1162 (υ PhO), 1109 (υ aliphatic C-O).

2.3.1.2 Synthesis of (4-((2-Hydroxy-4-*n*-alkoxy) benzylidene) amino)phenyl)ethanone.

Dissolve 2-Hydroxy4-n-alkoxybenzaldehyde (n = 2-8, 10, 12, 14, 16, 18, 10 mmol) and 4-aminoacetophenone (10 mmol) in minimal absolute ethanol, a few drops of glacial acetic acid was added and the reaction mixture was refluxed for 4 hours. Once cooled, a yellow crystal compound was isolated. The compound was filtered, washed with cool ethanol and vacuum dried **(Scheme 1).**

(4-((2-Hydroxy-4-(*n*-octyloxy)benzylidene)amino)phenyl)ethanone (A8)

Yellowish solid; Yield 65%.^{1}H NMR (400 MHz , $CDCl_3$, TMS) δ_H 13.45 (s, ArO**H**, 1H), 8.56 (s, -C**H**=N-, 1H), 8.04 (d, Ar**H**, 2H, *J* =4.8 Hz), 7.34-7.28 (m, Ar**H**,3H), 6.54-6.51 (dd, Ar**H**, 2H, *J* =7.2 Hz), 4.03 (t, -OC**H$_2$**-, 2H), 2.64 (s, -COC**H$_3$**, 3H), 1.85-1.30 (m, -O-C-(C**H$_2$**)$_6$-, 12H), 0.91-0.87 (t, -C-C**H$_3$**, 3H); IR (υ_{max}, cm^{-1}, KBr): 3421 (υOH), 2953, 2924, 2854 (υ aliphatic C-H), 1676 (υC=O), 1623 (υC=N), 1595, 1568 (υ aromatic C=C), 1198, 1171 (υ PhO), 1119 (υ aliphatic C-O).

(4-((2-Hydroxy-4-(*n*-decyloxy)benzylidene)amino)phenyl)ethanone (A10)

Yellowish solid; Yield 75% ; Mass (ES): m/z $[M+H]^+$ = 396.45; ^{1}H NMR (400 MHz , $CDCl_3$, TMS) δ_H 13.44 (s, ArO**H,** 1H), 8.57 (s, -C**H**=N-, 1H), 8.04 (d, Ar**H**, 2H, *J* =8.4 Hz), 7.33-7.28 (m,Ar**H**,3H), 6.53-6.51 (dd, Ar**H**2H, *J* =6.8 Hz), 4.02 (t, -OC**H$_2$**-, 2H), 2.64 (s, -COC**H$_3$**, 3H), 1.85-1.27 (m, -O-C-(C**H$_2$**)$_8$-, 16H), 0.91-0.87 (t, -C-C**H$_3$**, 3H); ^{13}C NMR (100 MHz , $CDCl_3$, TMS) δ_C 197.1, 164.2, 164.1, 162.8, 152.7, 134.8, 133.9, 129.9, 121.1, 112.7, 101.5, 68.3, 31.9, 29.5, 29.3, 29.3, 29.0, 26.6, 26.0, 22.7, 14.1; IR (υ_{max}, cm^{-1}, KBr): 3420 (υOH), 2954, 2921, 2851 (υ aliphatic C-H), 1676 (υC=O), 1624 (υC=N), 1595, 1569 (υ aromatic C=C), 1198, 1171 (υ PhO), 1119 (υ aliphatic C-O).

(4-((2-Hydroxy-4-(*n*-hexadecyloxy)benzylidene)amino)phenyl)ethanone (A16)

Yellowish solid; Yield 72%.^{1}H NMR (400 MHz ,$CDCl_3$,TMS) δ_H 13.44 (s, ArO**H**, 1H), 8.56 (s, -C**H**=N-, 1H), 8.03 (d, Ar**H**, 2H, *J* =8.4 Hz), 7.34-7.29 (m, Ar**H**, 3H), 6.55-6.52 (dd, Ar**H**, 2H, *J* =7.2 Hz), 4.03 (t, -OC**H$_2$**-, 2H), 2.65 (s, -COC**H$_3$**, 3H), 1.86-1.45 (m, -O-C-(C**H$_2$**)$_{14}$-, 28H), 0.91-0.87 (t, -C-C**H$_3$**, 3H); IR (υ_{max}, cm^{-1}, KBr): 3443 (υOH), 2918, 2848 (υ aliphatic C-H), 1676 (υC=O), 1623 (υC=N), 1596, 1569 (υ aromatic C=C), 1198, 1171 (υ PhO), 1118

(υ aliphatic C-O).

(4-((2-Hydroxy-4-(*n*-octadecyloxy)benzylidene)amino)phenyl)ethanone(A18)

Yellowish solid; Yield 70%; ^{1}H NMR (400 MHz ,$CDCl_3$,TMS) δ_H 13.44 (s, ArO**H**, 1H), 8.57 (s, -C**H**=N-, 1H), 8.04 (d, Ar**H**, 2H, *J* =6.8 Hz), 7.34-7.29 (m, Ar**H**, 3H), 6.54-6.52 (dd, Ar**H**, 2H, *J* =6.8 Hz), 4.03 (t, -OC**H$_2$**-, 2H), 2.65 (s, -COC**H$_3$**, 3H),1.86-1.44 (m,-O-C-(C**H$_2$**)$_{16}$-, 32H), 0.91-0.87 (t, -C-C**H$_3$**, 3H); ^{13}C NMR (400 MHz , $CDCl_3$, TMS) δ_C 197.1, 164.2, 164.1, 162.8, 152.7, 134.8, 133.9, 129.9, 121.1, 112.7, 108.1, 101.5, 68.3, 31.9, 29.7, 29.6, 29.6, 29.5, 29.3, 29.0, 26.6, 26.0, 22.7, 14.1; IR (υ_{max}, cm^{-1}, KBr): 3447 (υOH), 2918, 28148 (υ aliphatic C-H), 1676 (υC=O), 1623 (υC=N), 1596, 1570 (υ aromatic C=C), 1198, 1172 (υ PhO), 1118 (υ aliphatic C-O).

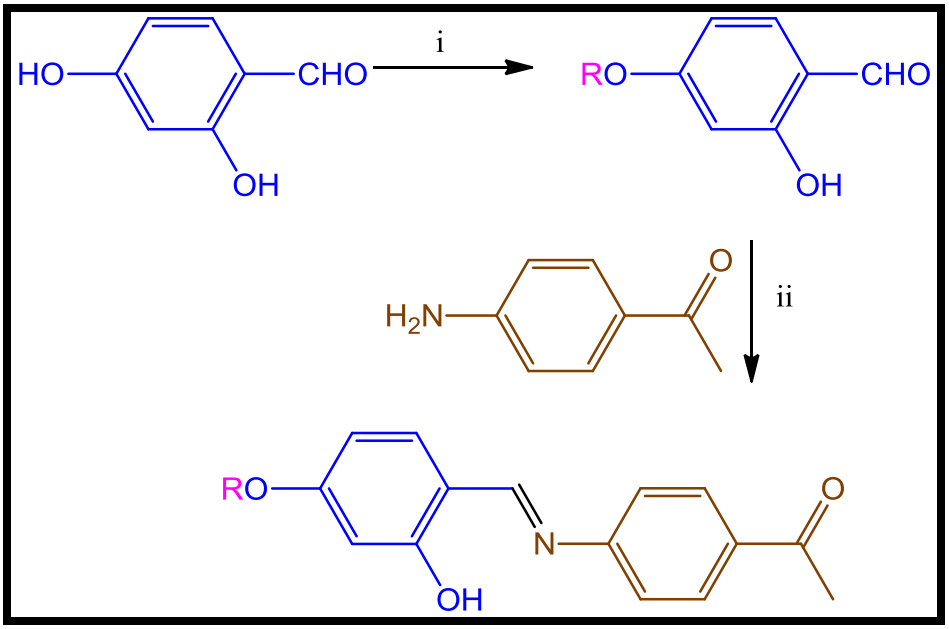

Where R = C_nH_{2n+1}; n = 2 to 8, 10, 12, 14, 16, 18.

Reagents and reaction conditions: i) RBr, $KHCO_3$, KI, dry acetone, reflux 24 hr, ii) glacial AcOH, absolute EtOH, reflux 4 hr.

Scheme 1.Synthesis protocol of series-A

2.3.2 Synthesis of Series-B

2.3.2.1 Synthesis of Cu(II) complex

The preparation of the Cu (II) complex is as follows.

Dissolve hydrated copper (II) acetate (2 mmol) in a minimum amount of ethanol, and add this solution to the hot ethanol solution of the ligand (n = 2 - 8, 10, 12, 14, 16, 18, 4 mmol). The reaction mixture was refluxed for 4 hours, during which a crystalline solid formed, which was filtered off, washed with hot distilled water, then washed with ethanol and dried under vacuum **(Scheme 2).**

Bis(2-((E)-((4-acetylphenyl)imino)methyl)-5-(*n*-octyloxy)phenoxy)copper (B8)

Brownish solid; Yield 80%; Mass (ES): m/z [M+2]+ 796.31; IR (υ_{max}, cm^{-1}, KBr): 2925, 2855 (υ aliphatic C-H), 1680 (υC=O), 1610 (υC=N), 1591, 1533 (υ aromatic C=C), 1205 (υ PhO), 1124 (υ aliphatic C-O), 597 (υM-N), 461 (υM-O); Conductance: 5 $ohm^{-1}cm^{2}mol^{-1}$

Bis(2-((E)-((4-acetylphenyl)imino)methyl)-5-(*n*-decyloxy)phenoxy)copper (B10)

Brownish solid; Yield 82%; IR (υ_{max}, cm^{-1}, KBr): 2922, 2852 (υ aliphatic C-H), 1680 (υC=O), 1610 (υC=N), 1592, 1533 (υ aromatic C=C), 1206 (υ PhO), 1123 (υ aliphatic C-O), 608 (υM-N), 461 (υM-O).

Bis(2-((E)-((4-acetylphenyl)imino)methyl)-5-(*n*-hexadecyloxy)phenoxy)copper (B16)

Brownish solid; Yield 75%; IR (υ_{max}, cm^{-1}, KBr): 2918, 2850 (υ aliphatic C-H), 1679 (υC=O), 1610 (υC=N), 1591, 1532 (υ aromatic C=C), 1205 (υ PhO), 1125 (υ aliphatic C-O), 610 (υM-N), 461 (υM-O); Conductance: 8 $ohm^{-1}cm^{2}mol^{-1}$

Bis(2-((E)-((4-acetylphenyl)imino)methyl)-5-(*n*-octadecyloxy)phenoxy)copper (B18)

Brownish solid; Yield 78%; IR (υ_{max}, cm^{-1}, KBr): 2918, 2850 (υ aliphatic C-H), 1679 (υC=O), 1609 (υC=N), 1591, 1533 (υ aromatic C=C), 1205 (υ PhO), 1124 (υ aliphatic C-O), 610 (υM-N), 461 (υM-O).

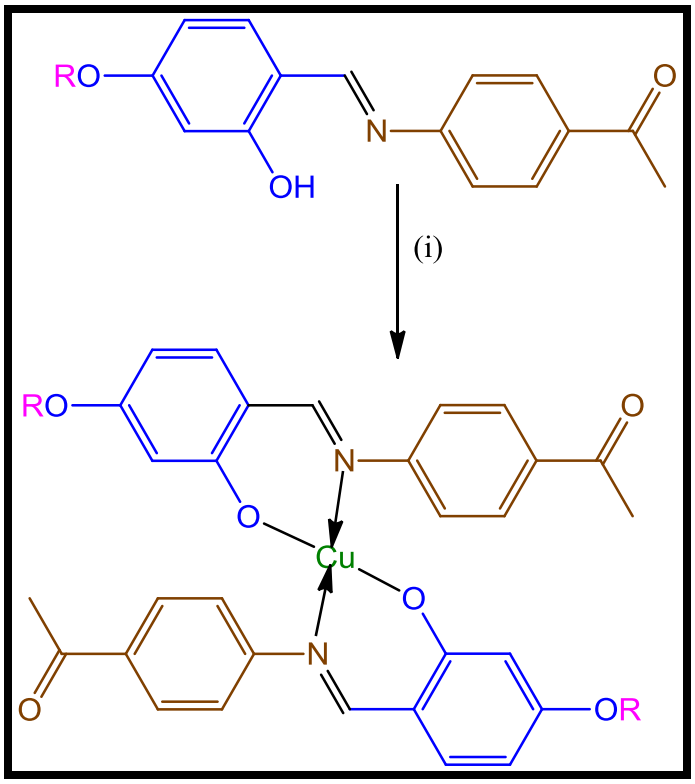

Where R = C_nH_{2n+1}; n = 2 to 8, 10, 12, 14, 16, 18.

Reagents and reaction conditions: i) $Cu(COOCH_3)_2.H_2O$, absolute EtOH, reflux 3 hrs.

Scheme 2. Synthesis protocol of series-B

2.4 Results and discussion

2.4.1 Series-A

In this series, 12 new homologues (4-((4-*n*-alkoxy-2-hydroxybenzylidene) amino)phenyl)ethanone were synthesized and characterized by FTIR, ^{1}HNMR, and ^{13}CNMR spectroscopy. In the ^{1}H-NMR spectrum of series-A compounds, the ArOH was observed as a singlet at δ = 13.44ppm. The imine proton (-CH=N-) was observed at δ 8.56 as a singlet. The aromatic protons of the phenyl ring were observed in the range δ 6.51 to 8.05 ppm. The (-OCH_2-) alkoxy protons were appeared at δ 4.04 as a triplet. The protons of the methyl group (-$COCH_3$) are observed at δ 2.65 as a singlet. The other alkoxy (-CH_2) protons are found in between δ 1.86-1.27 as a multiplet. Protons from the terminal methyl group are observed at δ 0.91 ppm as a triplet. The formation of Schiff's base is confirmed by the presence of characteristic sharp peak of imine hydrogen (H-C=N) at δ 8.56 ppm and disappearance of a characteristic peak of benzaldehyde hydrogen (H-C=O) at δ 9.71 ppm. .

In the ^{13}C-NMR spectrum of series-A compounds, carbonyl carbon was observed at δ 197.1 ppm. The peak appeared at δ 162.8 ppm corresponds to imine carbon (-CH=N). The aromatic carbons were observed in between δ 164.2-101.5 ppm. The carbon attached to alkoxy oxygen was observed at δ 68.3 ppm. The methyl carbon (-$COCH_3$) was appeared at δ 26.6 ppm. Other alkoxy chain carbons were found to be in the range δ 31.9 to 22.7 ppm. The ESI-Mass spectra of one of the homolog **A10** $[M + H]^+$ peak obtained at m/z 396.45 confirmed the structure of the molecule.

In the FT-IR spectrum, the characteristic peak of the acetophenone carbonyl group was observed at 1676 cm^{-1}. The compounds showed bands around 1623-1624 cm^{-1} corresponding to (υC=N).

The experimental results of TG-DTA show that there is no mass loss up to 260 ^{o}C, indicating the thermal stability of the synthetic compounds **(Figure 12).**

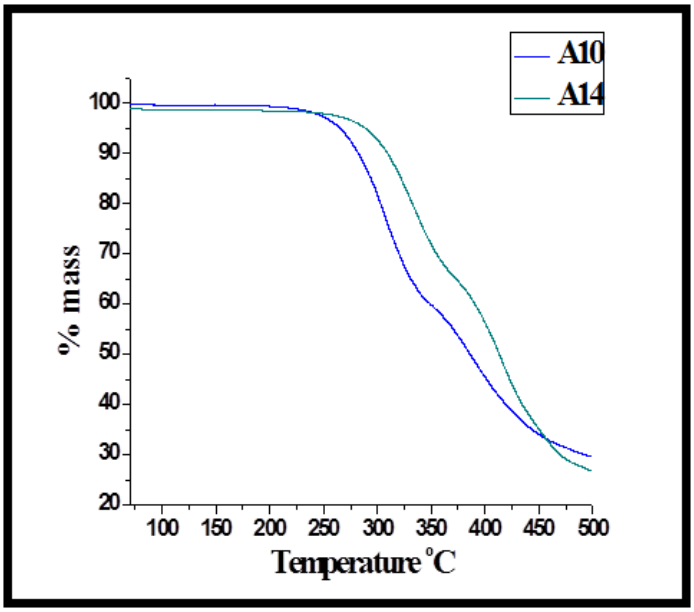

Figure 12. TGA thermogram of compound **A10** and **A14**

A differential scanning calorimeter (DSC) and a polarized optical microscope (POM) were used to check the mesogenic properties of all synthetic compounds. **Table 1** shows both phase transition temperatures and phase transition enthalpy (ΔH Jg^{-1}) in ^{o}C. The POM image for compound **A8** is illustrated in **Figure 13.**

Series-A		
An	Heating	Cooling
A2	Cr 147.2 (11.52) I	I 127.0 (11.52) Cr
A3	Cr 131.2 (3.77) I	I 124.2 (1.58) SmA 102.2 (16.29) Cr 86.0 (3.77) Cr
A4	Cr 117.4 (14.72) SmA132.1(1.89) I	I 126.2 (1.89) SmA 74.9 (3.63) Cr
A5	Cr 94.9 (2.89) Cr103.8 (24.76) SmA 136.9 (1.63) I	I 130.8 (3.63) SmA 79.6 (17.23) Cr
A6	Cr 90.2 (3.15) Cr 99.5 (5.84) SmA 146.3 (0.50) I	I 135.4 (2.09) SmA 75.1 (19.02) Cr
A7	Cr 90.0 (7.98) Cr 99.4 (7.64) SmA 146.1(4.24) I	I 140.1(3.48) SmA 70.3 (11.10) Cr
A8	Cr 87.5 (2.12) Cr 95.8 (6.37) SmA 150.0 (0.95) I	I 143.4 (1.82) SmA 64.3 (13.37) Cr
A10	Cr 95.4 (26.91) SmA 149.9 (5.97) I	I 143.4 (1.21) SmA 81.1 (19.64) Cr
A12	Cr 99.2 (18.69) SmA 147.3(0.52) I	I 144.7 (1.65) SmA 84.2 (4.34) Cr
A14	Cr 105.7 (17.53) SmA 146.4 (4.07) I	I 137.6 (1.55) SmA 88.5 (27.91) Cr
A16	Cr 107.8 (26.91) SmA 145.8 (0.57) I	I 139.3 (4.59) SmA 97.6 (11.31) Cr
A18	Cr 66.6 (2.40) Cr 107.8 (19.34) SmA 133.3 (0.86) I	I 126.7 (0.96) SmA 98.3 (31.30) Cr

Table 1. Phase transition temperatures in ^{o}C along with transition enthalpy values (ΔH Jg^{-1}).

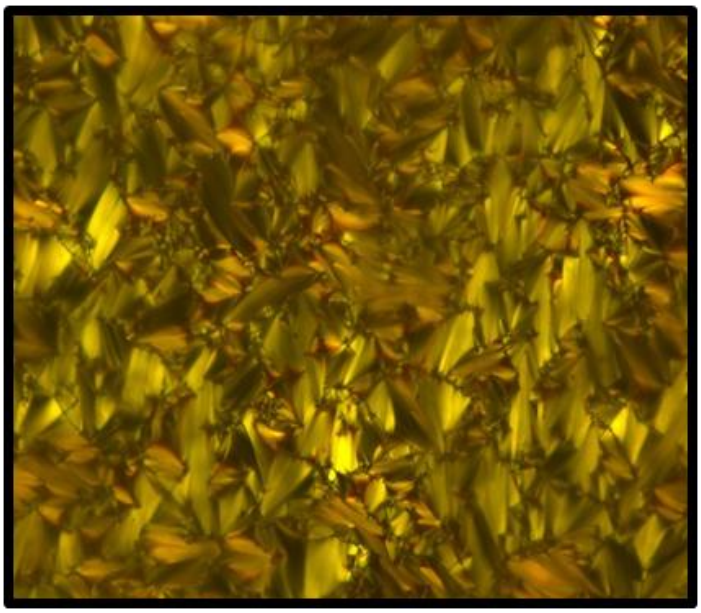

Figure 13. Fan-like texture of SmA phase **A8** on cooling at 143.4 ^{o}C

In the POM observation of compound **A2**, it melted directly from the crystal into an isotropic liquid, and did not show a liquid crystal phase. Subsequently, the DSC thermogram of compound **A2** showed only a single endothermal peak and an exothermal peak. The results of DSC and POM thus confirm that compound **A2** is not mesogenic. Due to the unfavorable value of the attractive force between anisotropic molecules, the non-mesogenic behavior of compound **A2** cannot withstand thermal oscillations, immediately destroys the crystal lattice and suddenly transforms into an isotropic liquid without an intermediate phase [21]. Compound **A3** is directly converted into an isotropic liquid when heated, but when cooled, it shows a fan-shaped optical texture of the smectic-A phase, indicating that it is monotropic. Furthermore, the DSC thermograph of **A3** confirms the monotropic nature. When heated, it shows an endothermic peak at 131.2°C, which corresponds to the melting point, and when cooled, it shows an exothermic peak at 124.2°C, 102.2°C and 86.0°C, corresponding to the isotropic liquid to SmA, SmA to crystals and crystal to crystal phase transitions **(Figure14).** Then, all members of the series-A from **A4** to **A18** have an enantiotropic smectic-A phase. Compound **A10** shows endothermic peaks at 95.4°C and 149.9°C, followed by exothermic peaks at 143.4°C and 81.1°C. The two endothermic peaks observed for this compound correspond to the crystal to SmA phase transition and SmA to isotropic liquid, and the two exothermic peaks show isotropic liquid to SmA and SmA to crystal transitions. As well, **A14** exhibits endothermic peaks at 105.7 °C and 146.4 °C, followed by exothermic peaks at 137.6 °C and 88.5 °C. The two endothermic peaks observed for this compound define the crystal to SmA and SmA to isotropic liquid transitions. The two exothermic peaks indicate the transition of the isotropic liquid to SmA and SmA to crystal. **Figure 14** depicts the DSC thermograms of the compound **A10** and **A14.**

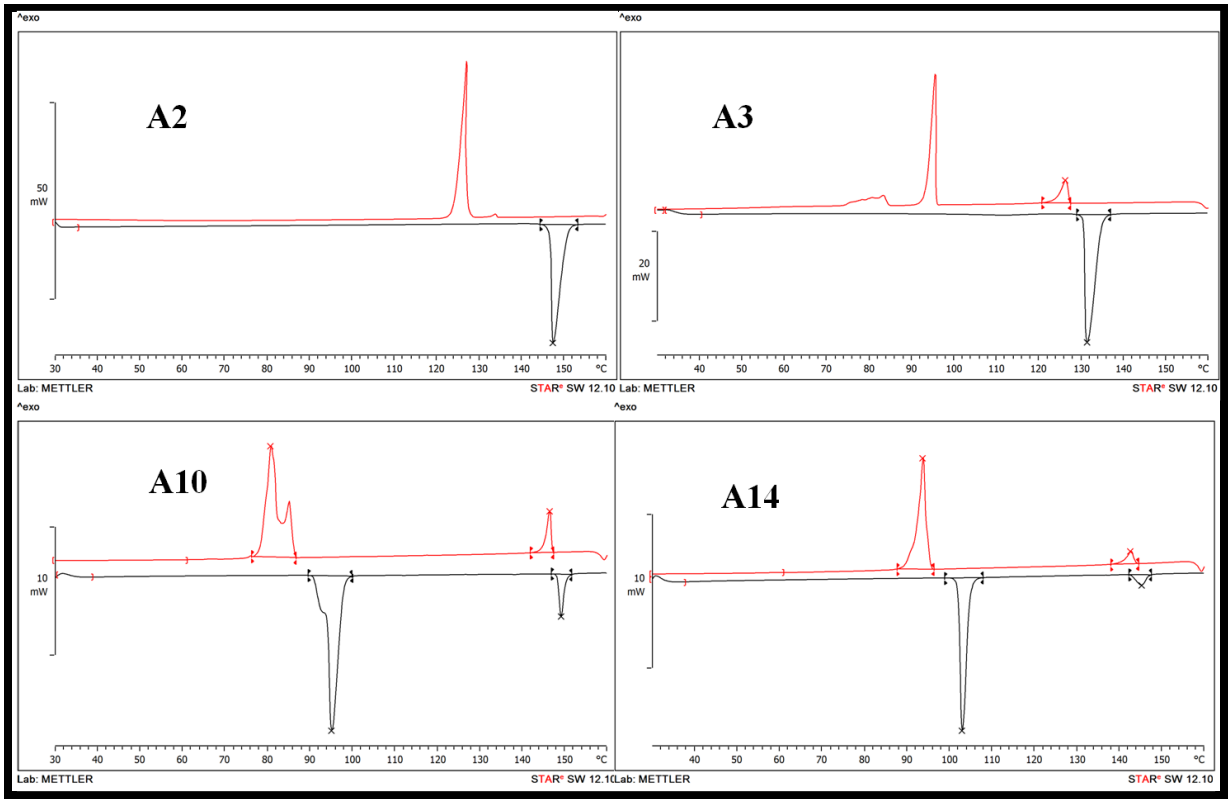

Figure 14. DSC thermogram of **A2, A3, A10 and A14**

Due to the favorable molecular rigidity and flexibility, the appropriate value of the anisotropic intermolecular attractive force promotes and stabilizes the accumulation of layered molecules in the crystal lattice to induce smectic properties. The absence of nematogenic mesophase formation in present series is attributed to end-to-end attraction is insufficient to maintain the statistically parallel orientation sequence of the floating molecules to induce nematic properties [22].

The relationship between the resulting transition temperature and the number of carbon atoms in the series is illustrated in **Figure 15**. The results indicate that the transition temperature trend for Cr to SmA decreases as the length of the terminal alkoxy chain increases up to a chain length 10, and then it increases as the length of the terminal alkoxy

chain increases. The clearing temperature increases as the chain length increases up to length 8, and then it decreases as the length of the terminal alkoxy chain increases. The sequential addition of a methylene unit contributes to molecular flexibility and the resulting comprehensive influence of molecular rigidity and flexibility, from one homologue to another, and leads to a reversal of the trend of mesogenic behavior [23].

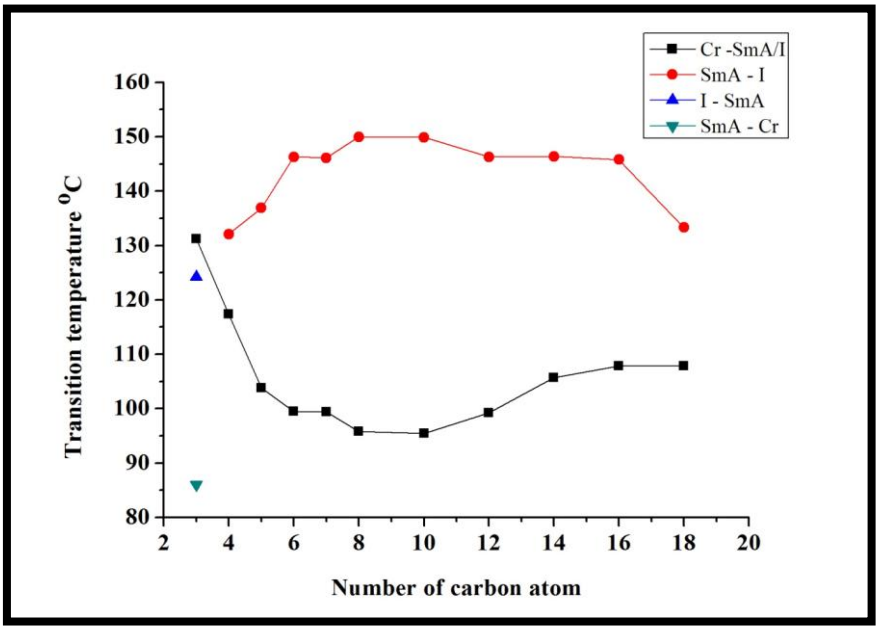

Figure 15. Dependence of transition temperatures on the increasing terminal alkoxy chain length

For homologous series, as a function of the increase in chain length in the cooling and heating cycles, the temperature range of the SmA phase as shown in **Figure 16**. In the cooling cycle, all compounds have a supercooling effect, which increases the SmA phase range. A compound with an alkyl chain length of 8 has the highest temperature range of the SmA phase during the cooling cycle.

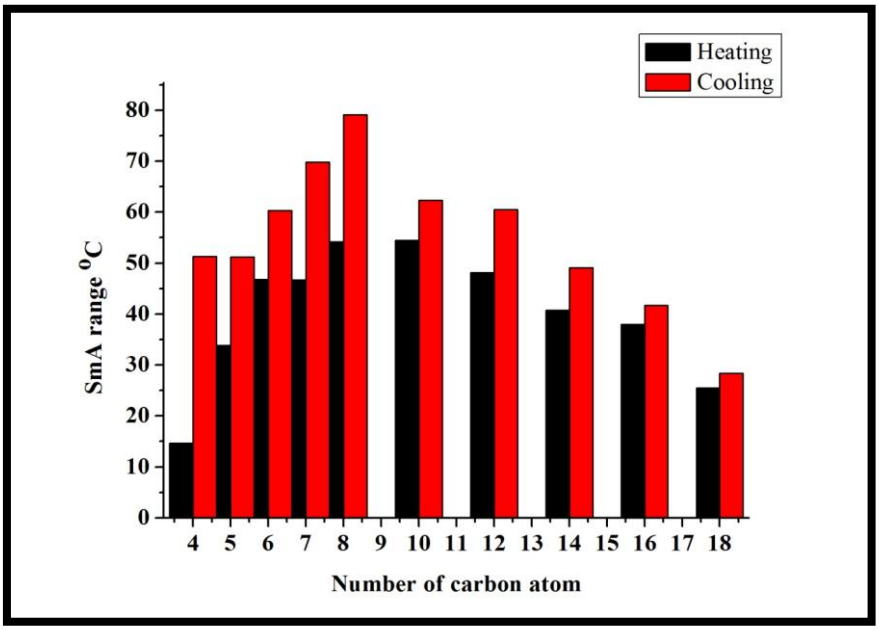

Figure 16. Temperature range of SmA phase transition

2.4.2 Series-B

In this series, 12 new Cu complexes of (4-((4-*n*-Alkoxy-2-hydroxybenzylidene) amino)phenyl)ethanone were synthesized and characterized by FT-IR.

In the FT-IR spectrum, for the metal complex, the characteristic peak of the carbonyl carbon of acetophenone group is found around 1679-1680 cm^{-1}. The metal complexes shows a band near 1609-1610 cm^{-1} which corresponds to (υC=N). Lowering in the peak of (υC=N) in metal complexes relative to ligand indicates the formation of the complex through N of azomethine group. In this series of metal complexes, due to the (υM-N) and (υM-O) vibrations, peaks at about 597-610 cm^{-1} and 410 cm^{-1} are obtained.

The electronic spectra of free ligands (**A8** and **A14**) and related copper complexes (**B8** and **B14**) in DMF from 280 to 480 nm are depicted in **Figure 17**. Electronic spectra of free ligands display band at 355 nm is attributed to π π* transition. The λ_{max} of free ligands in

copper complexes is red shifted to 375 nm. The bathochromic effect seen for the copper complexes arises due to the chelation by copper. The electronic spectra of Cu(II) complexes show an absorption band at 660-680 nm attributed dxy → dx^2-y^2 transition. The conductance values of complexes (section 2.3.2.1) clearly indicate their non-electrolyte behavior. The mass spectra of the **B8** (section 2.3.2.1) indicate the ML_2 type of complex, which are compatible with these complexes having square-planar structure.

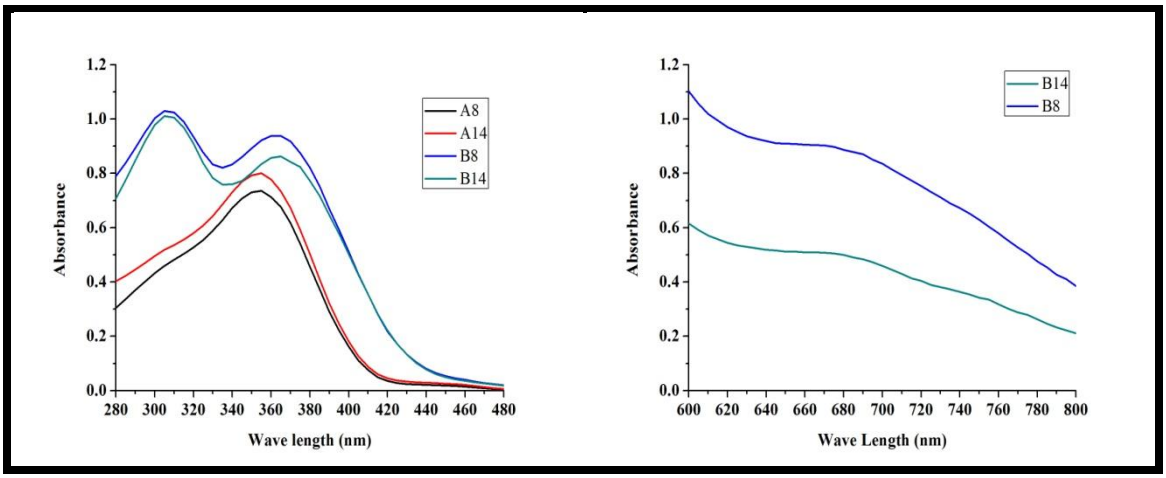

Figure 17. Electronic Spectra of ligands and complexes

The experimental results of TG-DTA show that there is no mass loss up to 260 ^{o}C, which indicates that the synthesized compound is thermally stable (**Figure 18**).

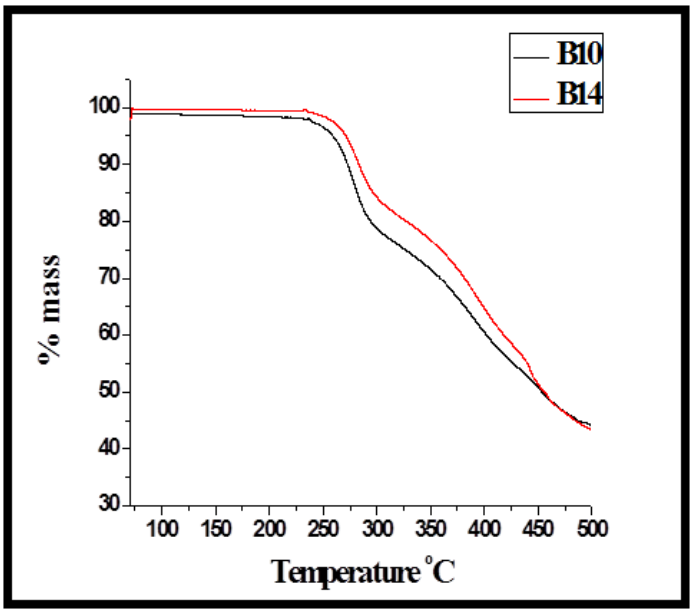

Figure 18. TGA thermogram of compound **B10** and **B14**

Mesomorphic properties of all synthesized complexes were investigated with a differential scanning calorimeter (DSC) and a polarizing optical microscope (POM). The phase transition temperatures in ^{o}C together with the transition enthalpy values (ΔH Jg^{-1}) are given in **Table 2**. The POM image of compound **B18** is depicted in **Figure 19**.

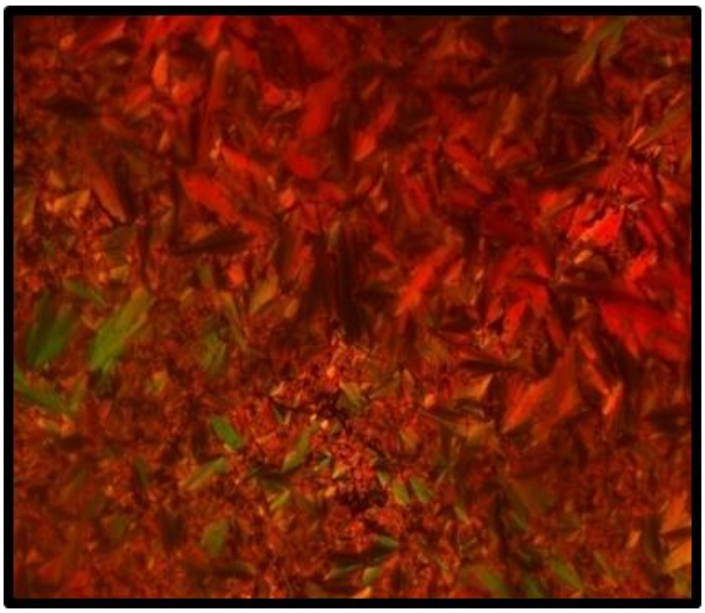

Figure 19. Fan-like texture of SmA phase **B18** on cooling at 212.5 ^{o}C

The thermal results of the complexes in **Table 2** show that **B2** to **B4** melted directly from the crystalline phase into an isotropic liquid. Compounds **B5** and **B6** become directly isotropic liquids when heated, but when cooled they show the typical fan-shaped optical texture of the SmA phase. Means monotropic, then all members of the series from **B7** to **B18** exhibit the enantiotropic SmA phase. The DSC thermogram of **B18** shows three transitions when heated, corresponding to crystal to crystal (128.4 ^{o}C); crystal to SmA (169.8°C) and SmA into an isotropic liquid transition (221.8°C), but no transition peak is found when cooling **(Figure 20).** The introduction of metal ions into the mesogenic ligand retains the mesogenic properties, but an increase in the mesogenic temperature is observed.

Series-B		
Bn	Heating	Cooling
B2	Cr 278.2 I	I 180.5 Cr
B3	Cr 271.0 I	I 175.3 Cr
B4	Cr 245.4 I	I 150.0 Cr
B5	Cr 223.2 (4.98) I	I 214.0 SmA 173.2 Cr
B6	Cr 228.3 (5.10) I	I 218.0 SmA 147.3 Cr
B7	Cr 197.1(1.60) SmA 226.7 (4.98) I	I 204.5 SmA 90.2 Cr
B8	Cr 183.6 (6.58) SmA 229.7 (5.26) I	I 200.4 SmA 70.0 Cr
B10	Cr 134.9 (2.28) Cr 179.8 (10.73) SmA 235.1 (6.58) I	I 183.6 SmA 75.0 Cr
B12	Cr 132.0 (0.39) Cr171.7(0.56) SmA234.1(1.94) I	I 228.6 SmA 101.2 Cr
B14	Cr 127.7 (8.70) Cr169.4 (3.36) SmA226.2 (5.61) I	I 210.5 SmA 114.0 Cr
B16	Cr 121.9 (0.91) Cr163.4 (1.35) SmA223.4 (1.51) I	I 205.0 SmA 104.3 Cr
B18	Cr 128.4 (6.45) Cr169.8 (5.85) SmA 221.8 (1.27) I	I 212.5 SmA 103.8 Cr

Table 2. Phase transition temperatures in ^{o}C, along with transition enthalpy values (ΔH Jg^{-1})

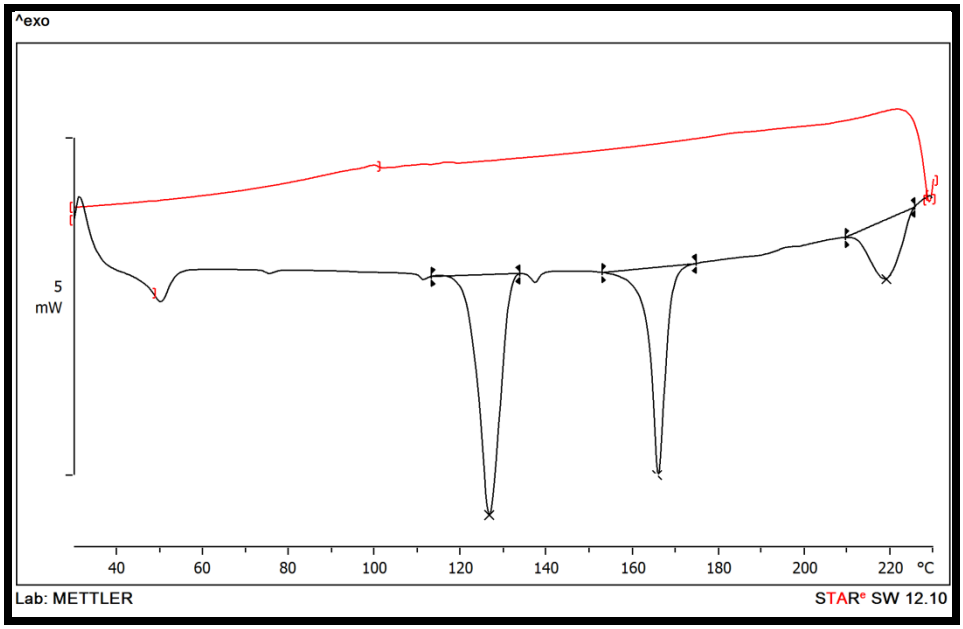

Figure 20. DSC thermogram of compound **B18**

The obtained transition temperature is plotted against the number of carbon atoms, as shown in **Figure 21.** It is found that in the metal complexes, the transition temperature for Cr to SmA decreases with the increase of the terminal alkoxy chain length up to 16, and then increases when the chain length is 18. Whereas temperature of the clearing point show rising tendency up to chain length 12 and then little levels off up to chain length 18.

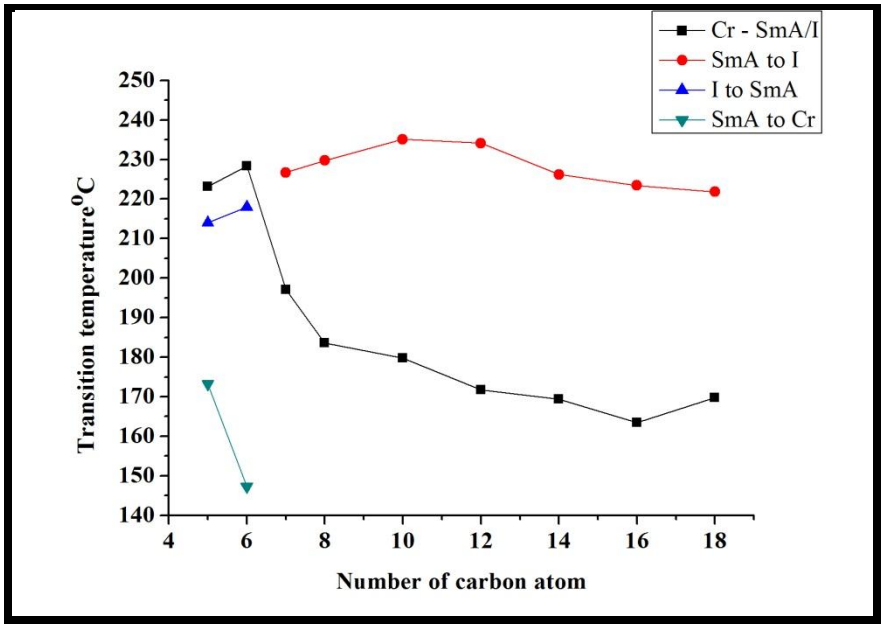

Figure 21. Dependence of transition temperatures on the increasing terminal alkoxy chain length

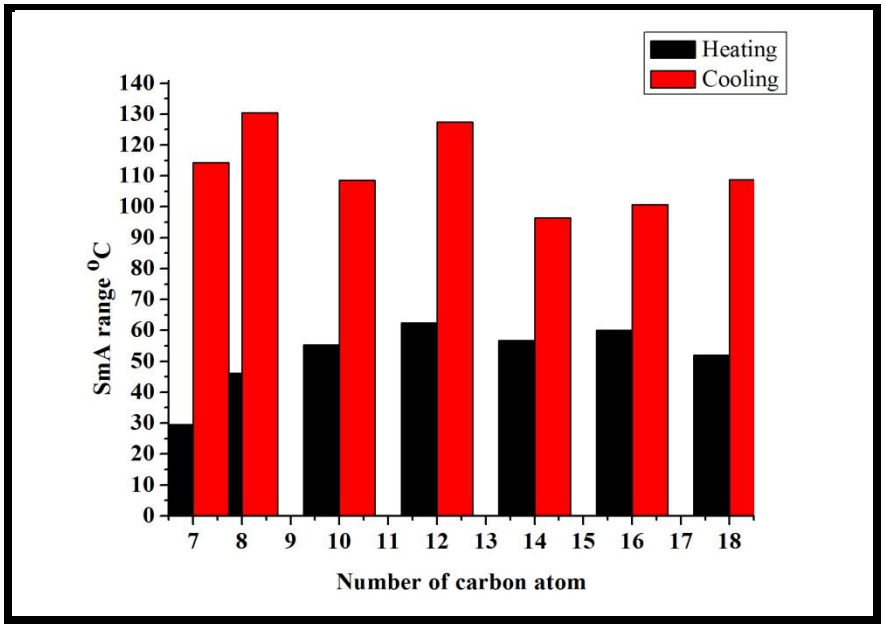

Figure 22. Temperature range of SmA phase transition

The change in the temperature range of the smectic A phase as a function of the increase in chain length during the cooling and heating cycles is shown in **Figure 22**. During the cooling cycle, all compounds have a supercooling effect, thus increasing the SmA phase range. In the homologous series, compounds with an alkyl chain length of 8 show the maximum temperature range of the SmA phase when cooled.

2.5 Structurally similar compounds.

Compare the mesogenic behaviors of compound **A10** from homologous series A and compound **B10** from homologous series B with other known compounds X [24] and compound Y [24] with similar structures; as shown in **Figure 23.**

The compound **A10** and compound X chosen for comparison are structurally identical with respect to two phenyl rings linked through –CH=N– central bridge that contribute to molecular rigidity and the left decyloxy terminal end group that contributes to the molecular flexibility. However, they differ with respect to right-sided terminal tail end functional groups–$COCH_3$ and –$COOCH_3$ whose polarity and polarizability creates difference in the magnitudes of mesomorphism and the degree of mesomorphism. **Figure 23** shows that the Sm-A mesophase length and Sm-A thermal stability of compound **A10** are higher by 30.4 ^oC and 11 ^oC, respectively, than for compound X. Similarly the Sm-A mesophase length and Sm-A thermal stability of compound **B10** are higher by 39.0 ^oC and 26.9 ^oC, respectively, than for compound Y. The molecular structures of compounds **A10** and X show that compound **A10** has a more polar –$COCH_3$ functional group compare to –$COOCH_3$ as a terminal end group. As a consequence of this compound A10 has a more intermolecular attraction compared to compound X and has shown greater stability [25].

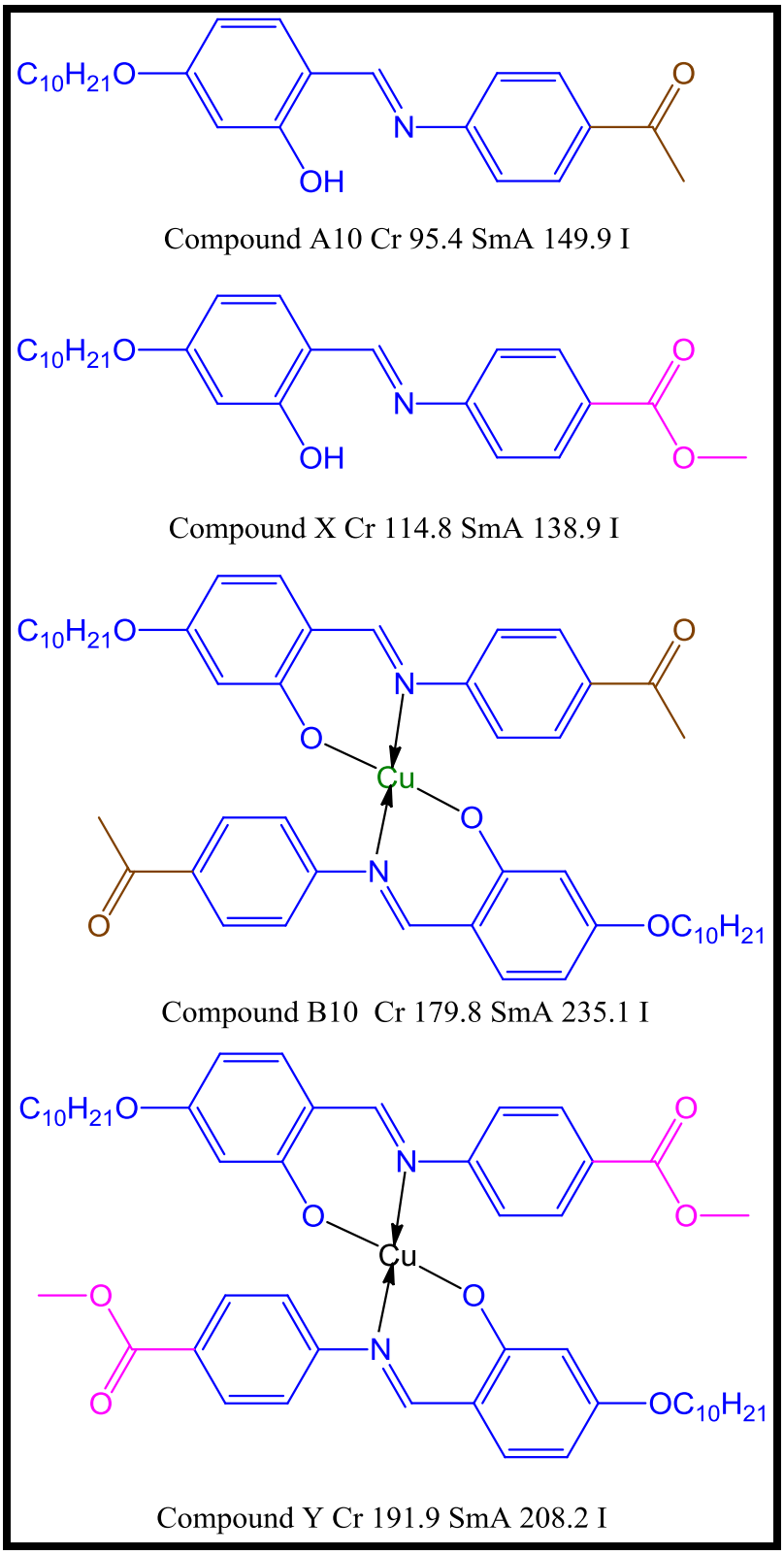

Figure 23. Structurally similar compounds to series-A and series-B

2.6 Conclusion

As a conclusion, two homologous series of ligand and Cu(II) complex were synthesized and characterized by FTIR, ^{1}HNMR, ^{13}CNMR and other analytical methods. The mesophase shown in the two series was studied by POM and confirmed by thermograms of DSC. Both series are purely smectogenic. In the homologous ligand series, the SmA intermediate phase starts with *n*-propoxy derivatives as monotropic, and then all members of the homologous ligand series show the enantiomeric behavior of SmA. In the Cu(II) metal complex series, the SmA mesophase starts with *n*-pentyloxy derivatives as monotropic, and *n*-hexyloxy derivatives also show monotropic nature. Meanwhile, the enantiotropic SmA mesophase exhibited from *n*-heptyloxy to *n*-octadecyloxy derivatives. A chain length of 8 shows the maximum temperature range of the SmA phase, in both series on cooling. Molecular flexibility and terminal end group difference can cause variations in mesomorphic behaviors of a substance.

2.7 References

[1] Giroud-Godquin A-M, Maitlis PM. Metallomesogens: Metal Complexes in Organized Fluid Phases. Angew. Chemie Int. Ed. English. 1991;30:375–402.

[2] Espinet P, Esteruelas MA, Oro LA, et al. Transition metal liquid crystals: advanced materials within the reach of the coordination chemist. Coord. Chem. Rev. 1992; 117: 215–274.

[3] Hudson SA, Maitlis PM. Calamitic metallomesogens: metal-containing liquid crystals with rodlike shapes. Chem. Rev.1993;93:861–885.

[4] Neve F. Metallomesogens. Synthesis, properties, and applications. Edited by J. L. Serrano, VCH, Weinheim 1996, xvii, 498 pp., hardcover, DM 298.00, ISBN 3-527-29296-9. Adv. Mater. 1996;8:864–866.

[5] Collinson SR, Bruce DW. Metallomesogens—Supramolecular Organization of Metal Complexes in Fluid Phases Perspect. Supramol. Chem. 1999. p. 285–369.

[6] Vorländer D. Verhalten der Salze organischer Säuren beim Schmelzen. Berichte der Dtsch. Chem. Gesellschaft 1910;43:3120–3135.

[7] Vorlander D. Die Erforschung der molekularen Gestalt mit Hilfe der kristallinischen Flüssigkeiten, Z. phys. Chem.1923;105:211.

[8] Chen C-J, Wang I-W, Sheu H-S, et al. Metallomesogens derived from benzoxazoles–salicylaldimine conjugates. Tetrahedron 2011;67:8120–8130.

[9] Binnemans K, Görller-Walrand C. Lanthanide-Containing Liquid Crystals and Surfactants. Chem. Rev. 2002;102:2303–2346.

[10] Heng B-T, Yeap G-Y, Mahmood WAK, et al. Alkyl chain self ordering, induction and suppression of mesophase by Cu(II) containing [1,2,3]-triazole-based bidentate salicylaldimine ligands: synthesis, characterisation and X-ray diffraction studies. Liq.

Cryst. 2014;41:1897–1910.

[11] Rezvani Z, Nejati K, Seyedahmadian M, et al. Investigation of Liquid Crystalline Behavior of Copper(II) Complexes Derived from Azo-Containing Salicylaldimine Ligands with Lateral Hydroxyl Group. Mol. Cryst. Liq. Cryst. 2008;493:71–81.

[12] Nejati K, Rezvani Z, Alizadeh E, et al. Synthesis and mesomorphic properties of symmetric tetradentate Schiff bases based on azo-containing salicylaldimines and their copper(II) complexes. J. Coord. Chem. 2011;64:1859–1870.

[13] Singh B, Singh MK, Dhar R, et al. Synthesis, Characterization and Mesomorphic Properties of n-(4-n-Alkoxy-2-Hydroxybenzylidene)-4-Carbethoxyaniline and their Copper Complexes. Mol. Cryst. Liq. Cryst. 2004;411:29–40.

[14] Date R, Bruce D. Discotic salicylaldimato metal complexes exhibiting columnar mesophases and their mixtures with rod-like salicylaldimato complexes. Liq. Cryst. 2004;31:1435–1444.

[15] Lai CK. Smectic bimetallomesogens: synthesis, characterization and mesomorphic properties and the crystal structure of bis[N-(3-hydroxypropyl)-4-octanoylsalicylaldiminato]copper(II) complex. Liq. Cryst. 1998;25:689–698.

[16] Bhattacharjee CR, Chakraborty S, Das G, et al. Emissive “zinc(II)-salphen” core: building block for columnar liquid crystals. Liq. Cryst. 2012;39:1435–1442.

[17] Gulbas HE, Ocak H, Gursel YH, et al. Synthesis and Mesomorphic Properties of New Side Chain Liquid Crystalline Oligomers Containing Salicylaldimine Mesogenic Groups. Mol. Cryst. Liq. Cryst. 2013;574:40–49.

[18] van Deun R, Binnemans K. Influence of the ligand structure on the liquid crystalline properties of lanthanide-containing salicylaldimine mesogens. Liq. Cryst. 2003;30:479–486.

[19] Prajapati AK, Bonde N. Synthesis of two naphthyl containing homologous series of mesogenic ligands and the related metallomesogens containing Cu(II). Liq. Cryst. 2006;33:1189–1197.

[20] Bhattacharjee CR, Datta C, Das G, et al. Green emissive salicylaldimine-based polar Schiff bases with short alkoxy tails and their copper(II)/oxovanadium(IV) complexes: Synthesis and mesomorphism. Liq. Cryst. 2012;39:373–385.

[21] Jain BB, Patel RB. Synthesis and mesomorphic behavior of liquid crystal chalconyl esters. Mol. Cryst. Liq. Cryst. 2016;633:63–71.

[22] Bhola GN, Bhoya UC. Mesomorphism dependence on heterocyclic end group. Mol. Cryst. Liq. Cryst. 2016;625:11–19.

[23] Marathe RB, Doshi A V. Study of relation between liquid crystal properties and molecular structure of halogenated benzyl alcohol ester derivative. Mol. Cryst. Liq. Cryst. 2017;648:14–21.

[24] Singh HK, Singh SK, Kumar V, et al. Synthesis, Characterization, and Mesomorphic Investigations of Calamitic Liquid Crystals – methyl 4-(4′-(alkoxy)-2-hydroxybenzylideneamino) benzoates and Their Copper(II) and Nickel(II) Complexes. Mol. Cryst. Liq. Cryst. 2013;587:1–17.

[25] Marcos M, Meléndez E, Ros MB, et al. Influence of Polar End Groups on Induced Smectic Phase Appearance. Mol. Cryst. Liq. Cryst. Inc. Nonlinear Opt. 1989;167:239–252.

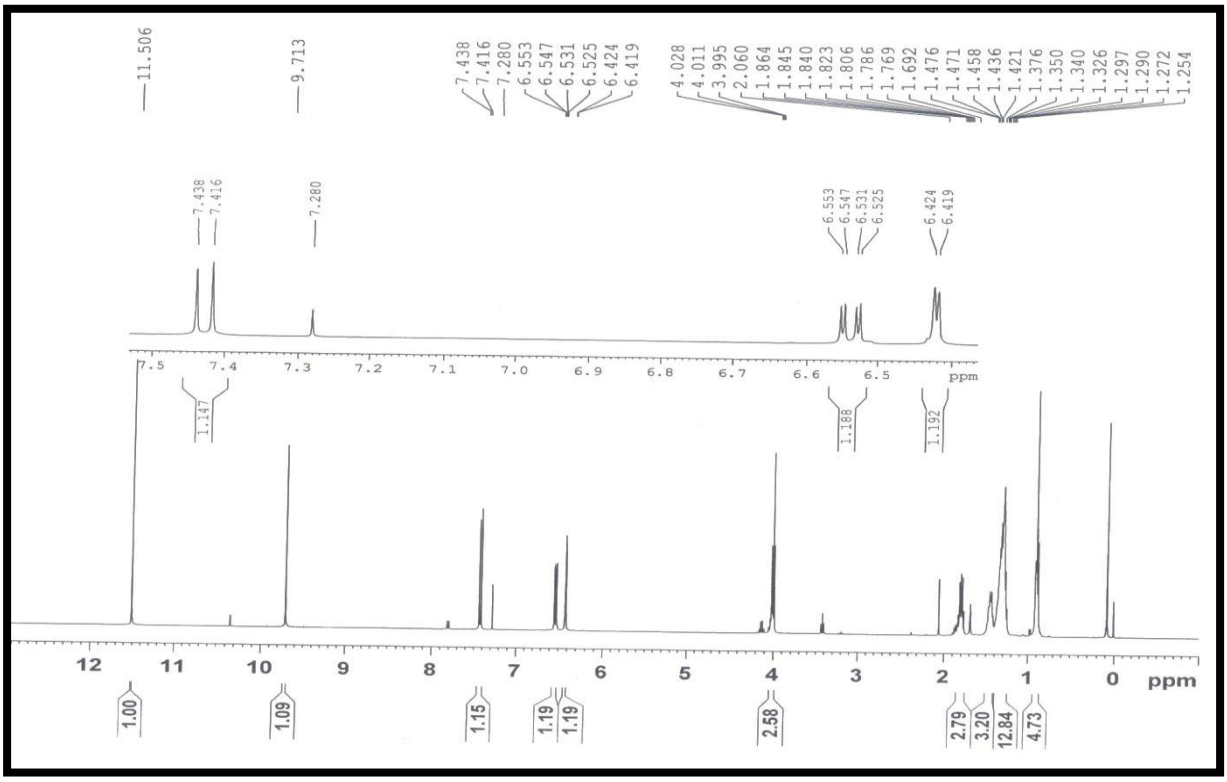

^{1}H NMR of 2-Hydroxy-4-(octyloxy)benzaldehyde

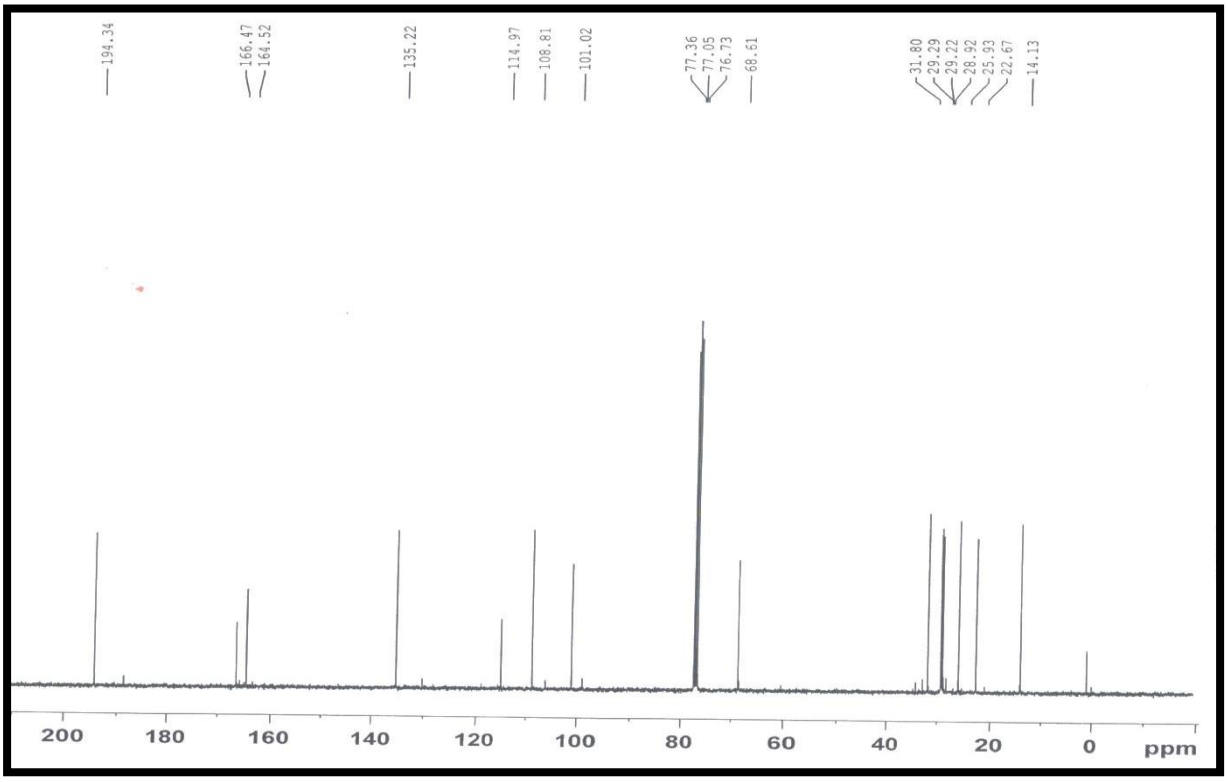

^{13}C NMR of 2-Hydroxy-4-(octyloxy)benzaldehyde

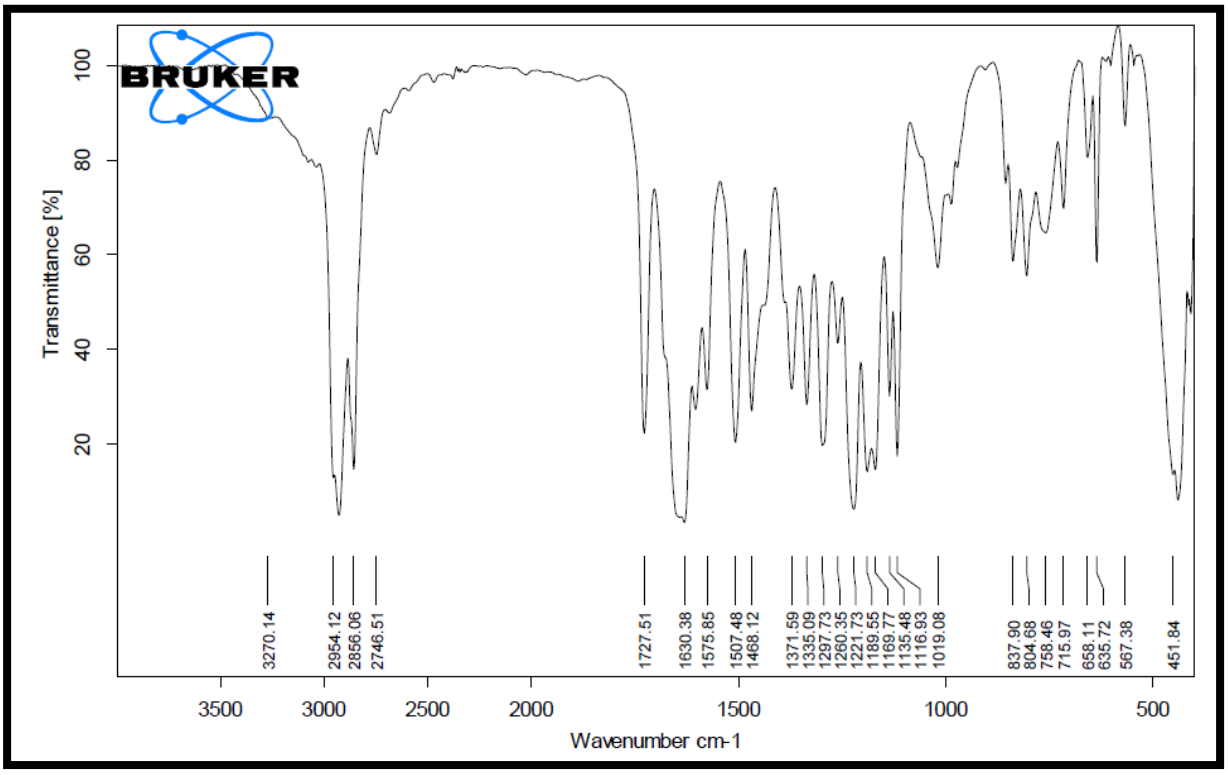

IR spectra of 2-Hydroxy-4-(octyloxy)benzaldehyde.

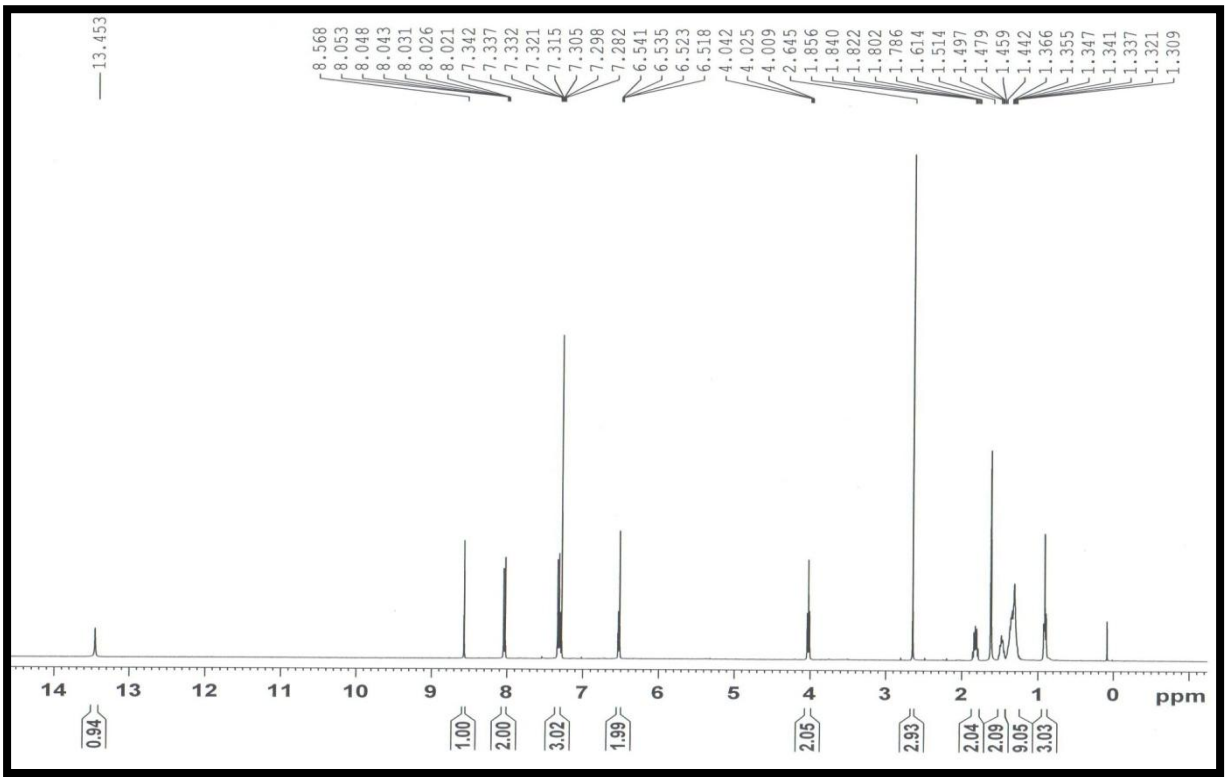

^{1}H NMR of A8

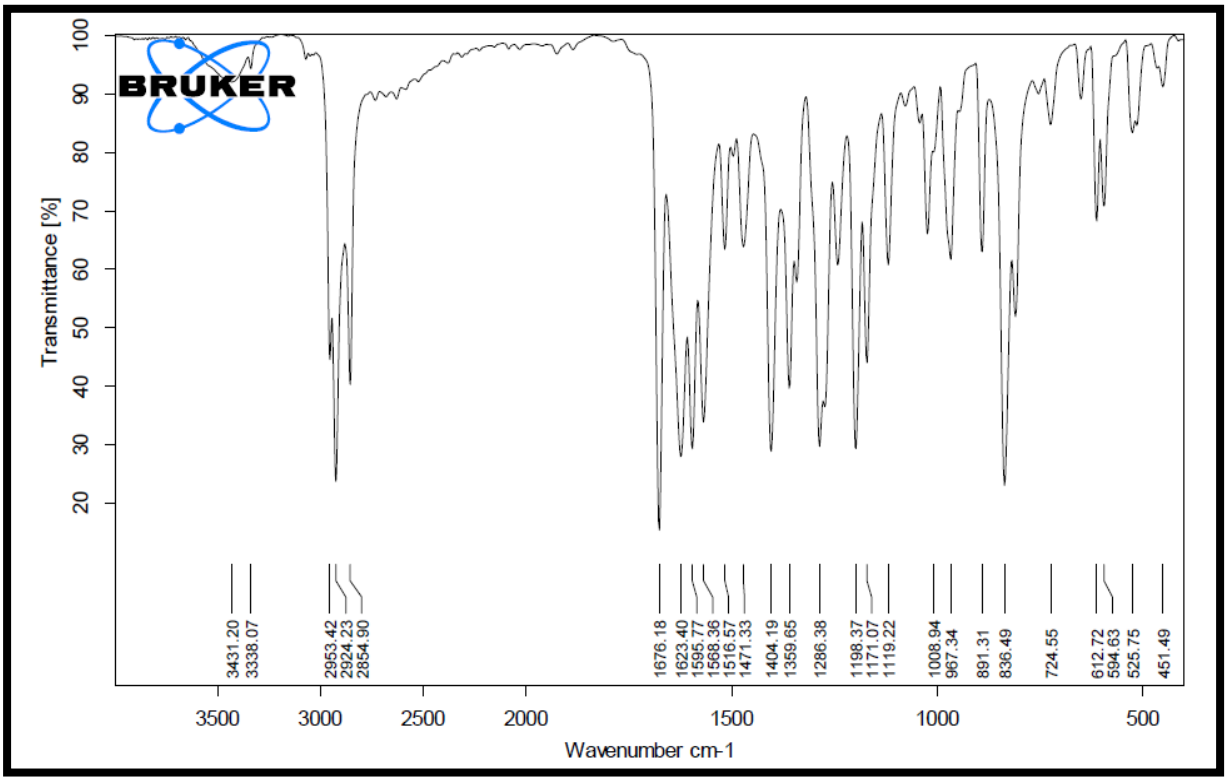

IR spectra of A8

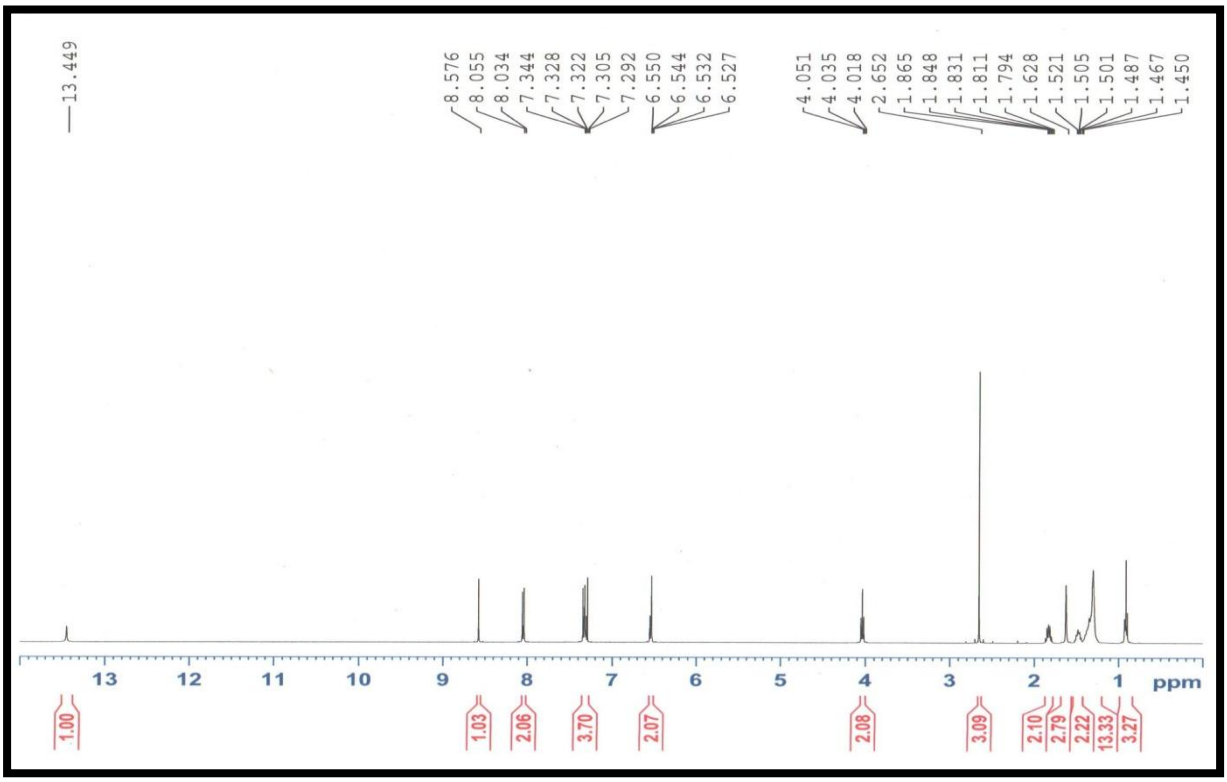

^{1}H NMR of A10

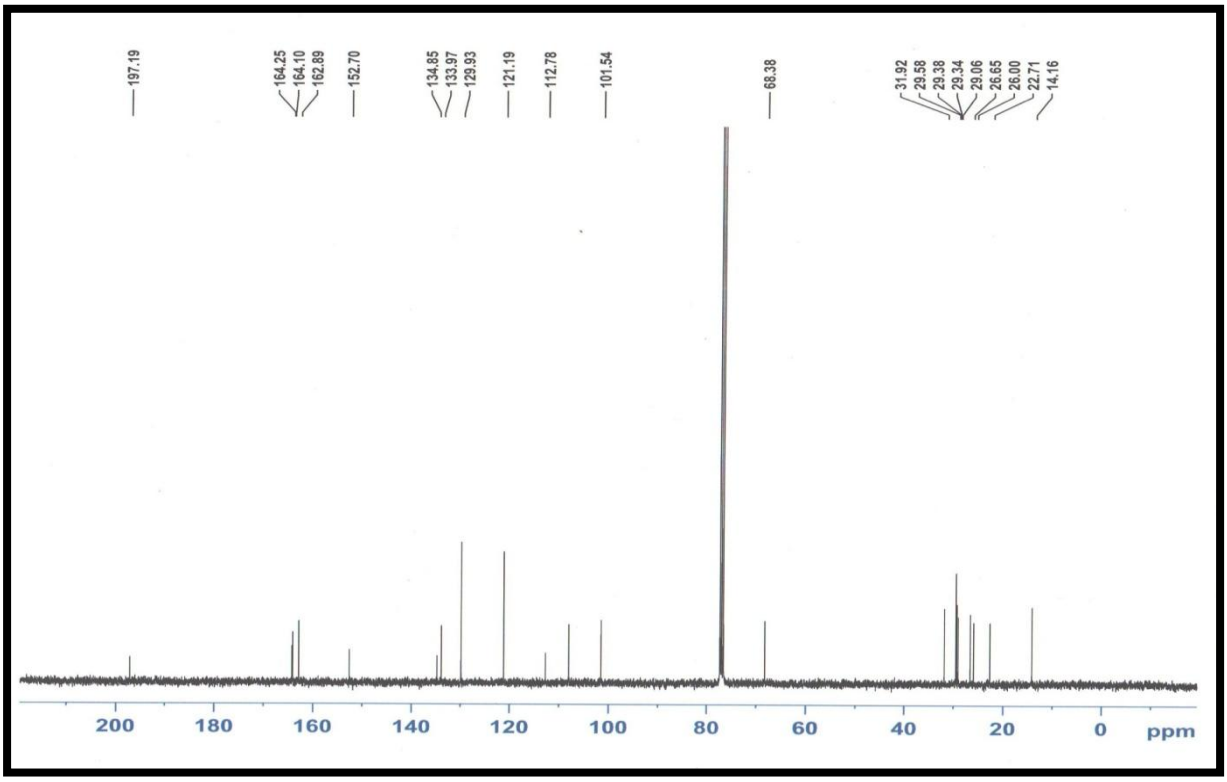

^{13}C NMR of A10

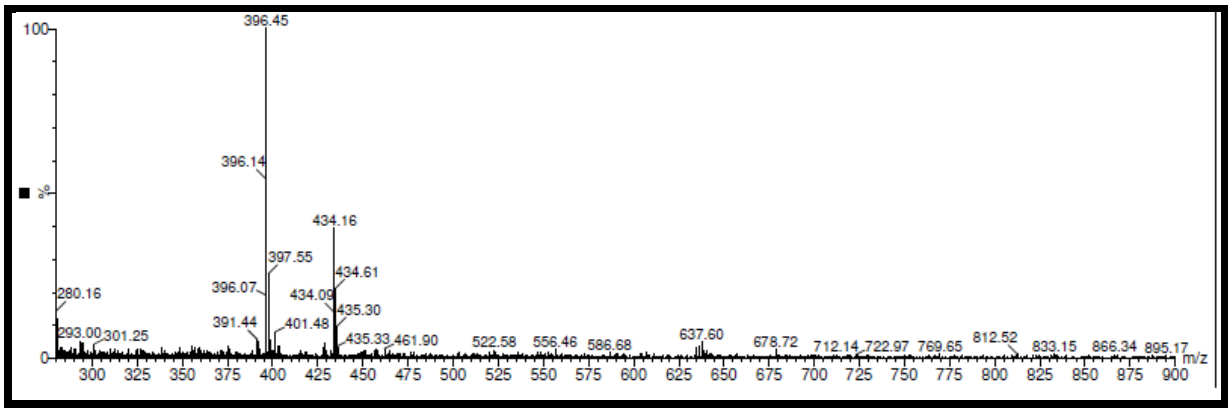

Mass spectra of A10

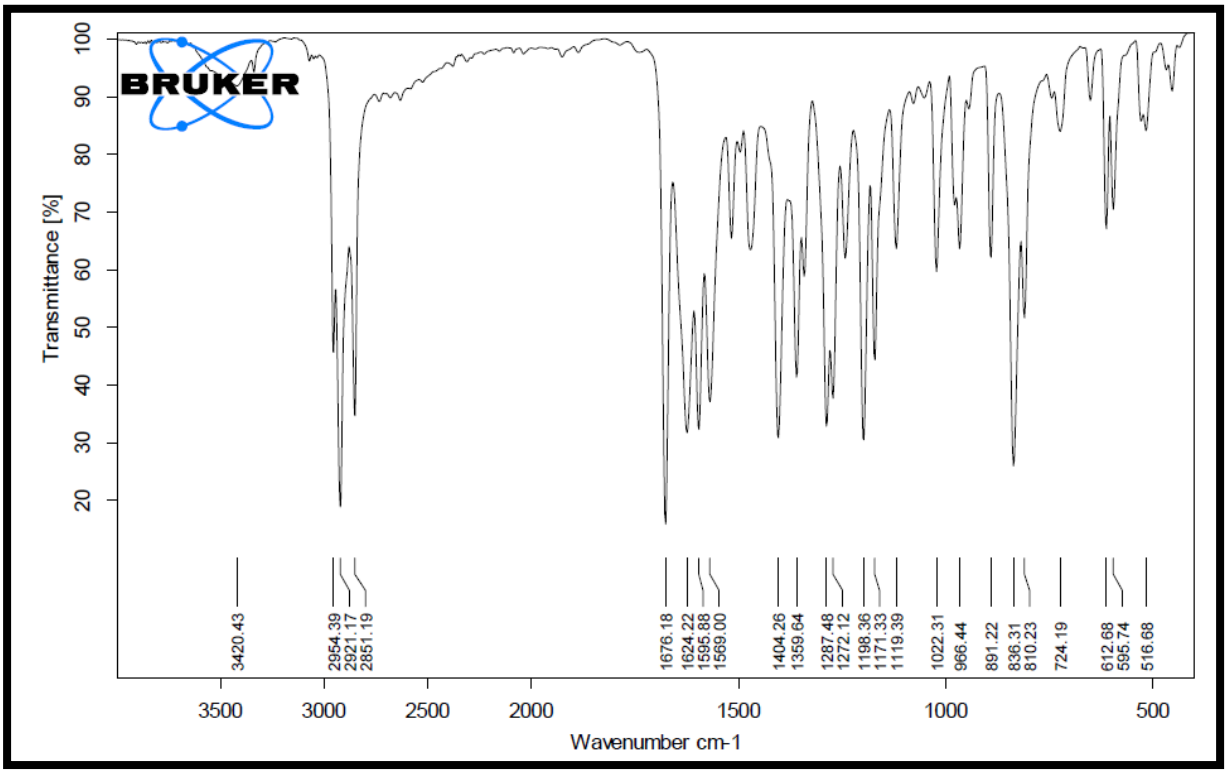

IR spectra of A10

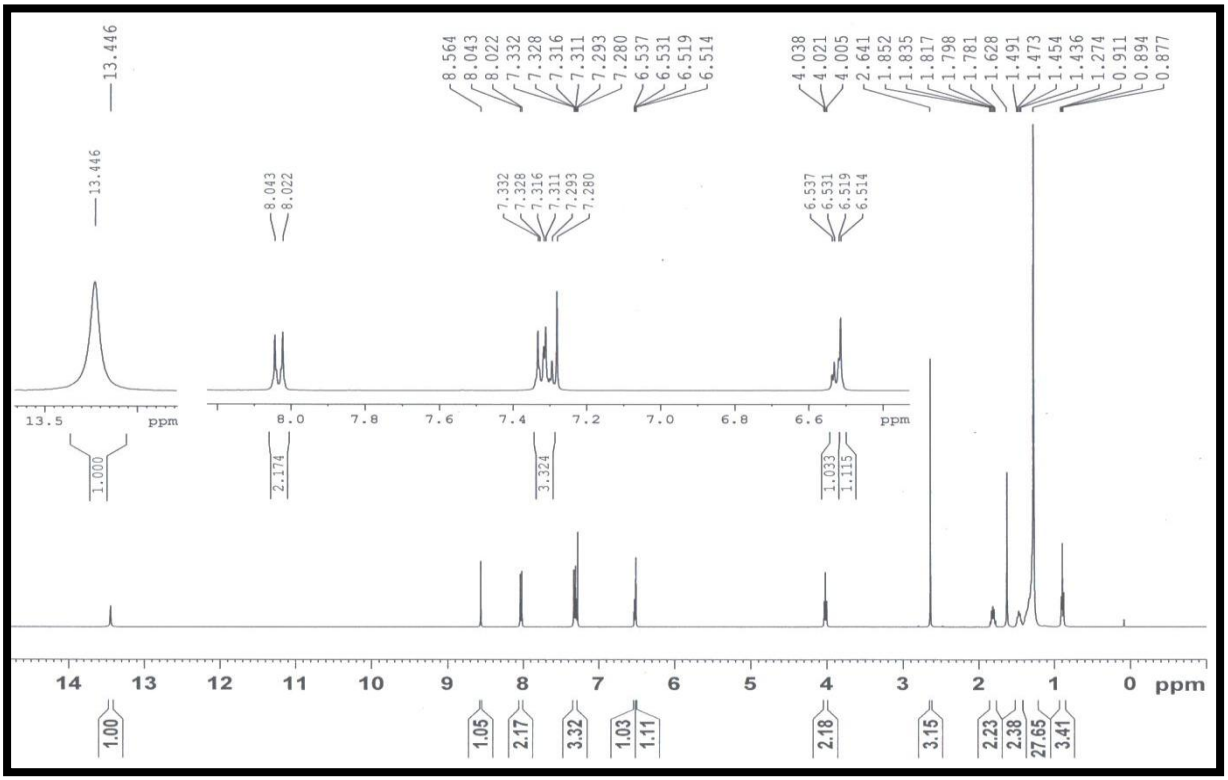

^{1}H NMR of A16

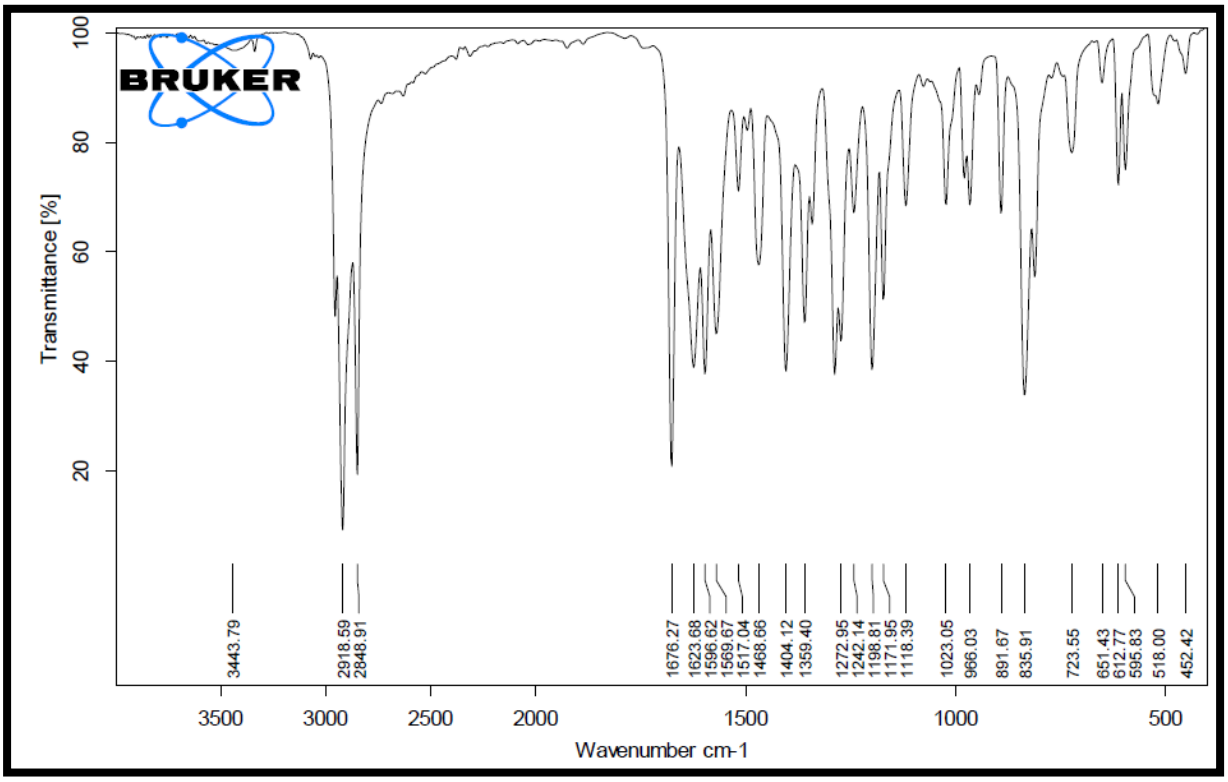

IR spectra of A16

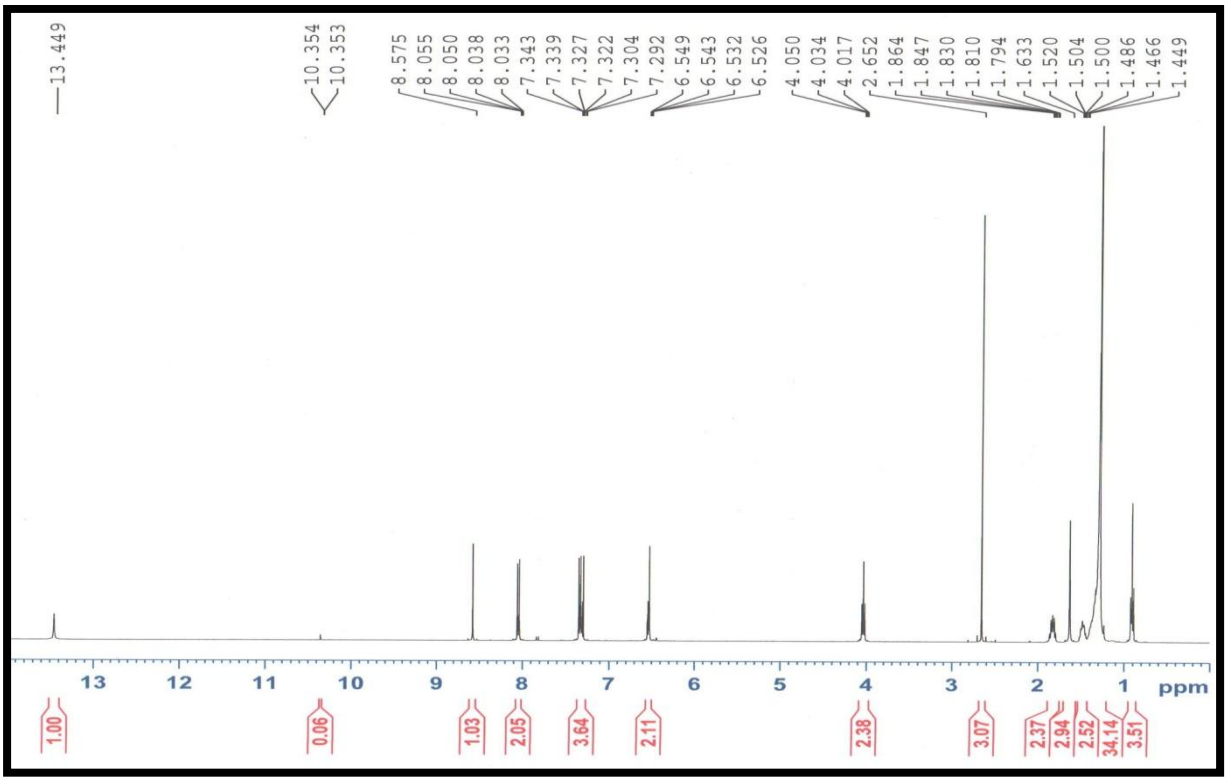

^{1}H NMR of A18

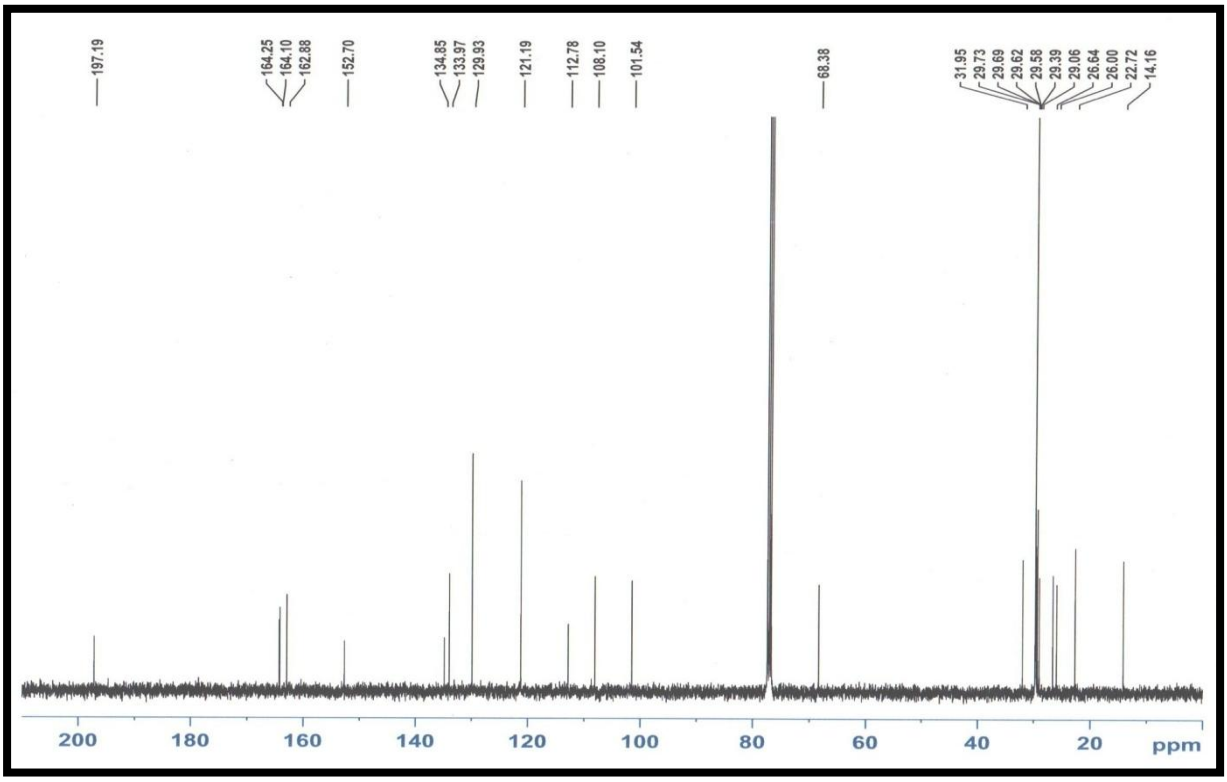

^{13}C NMR of A-18

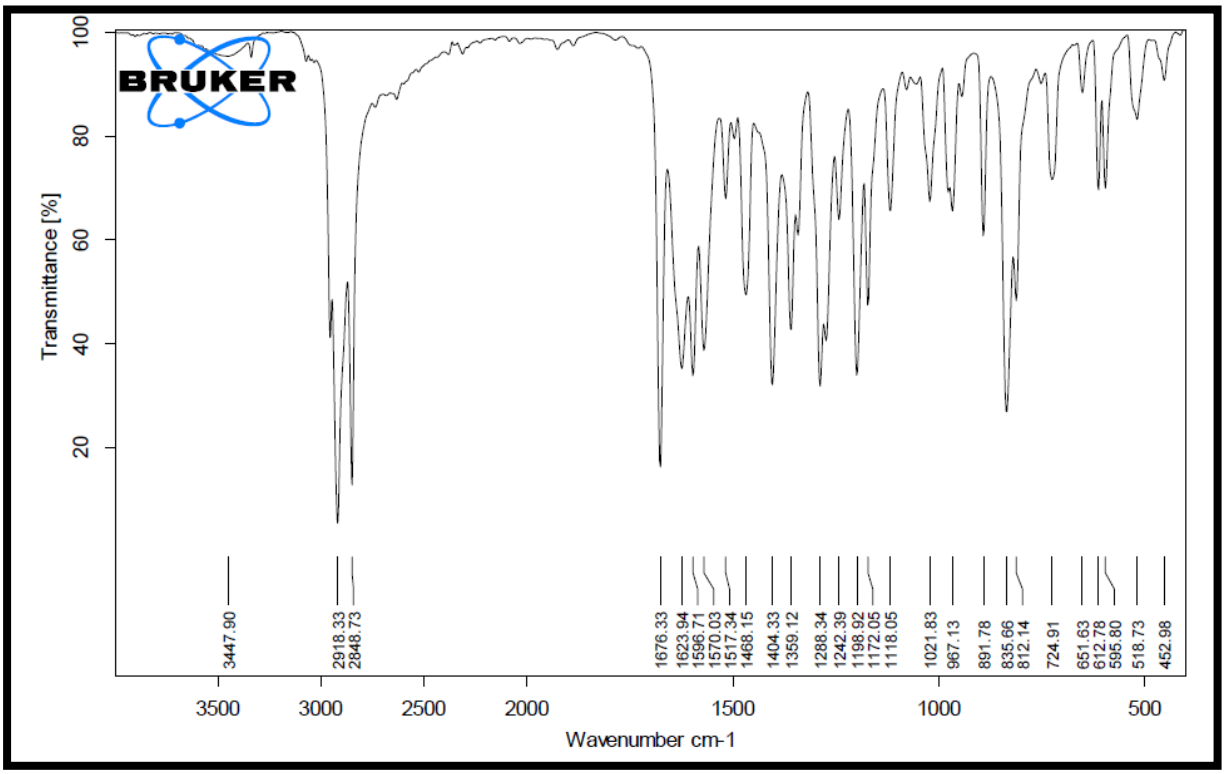

IR spectra of A18

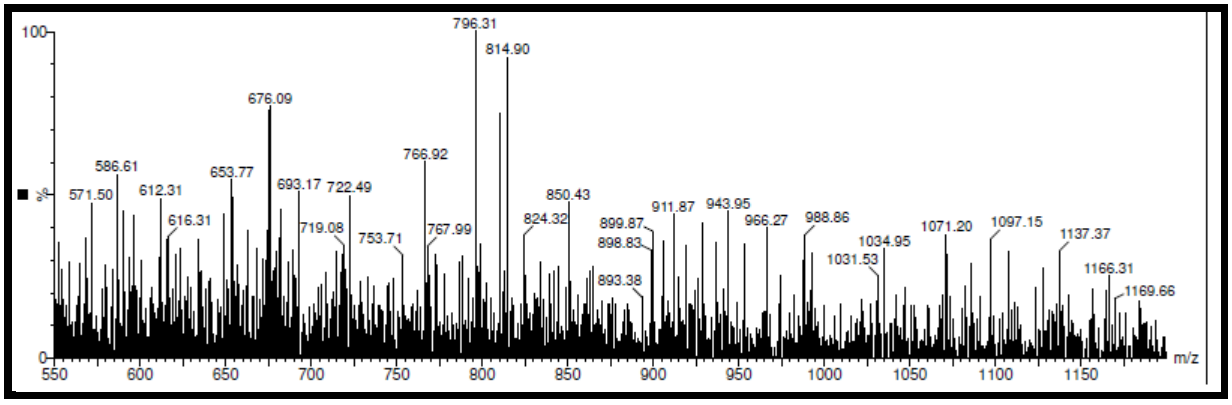

Mass spectra of B8

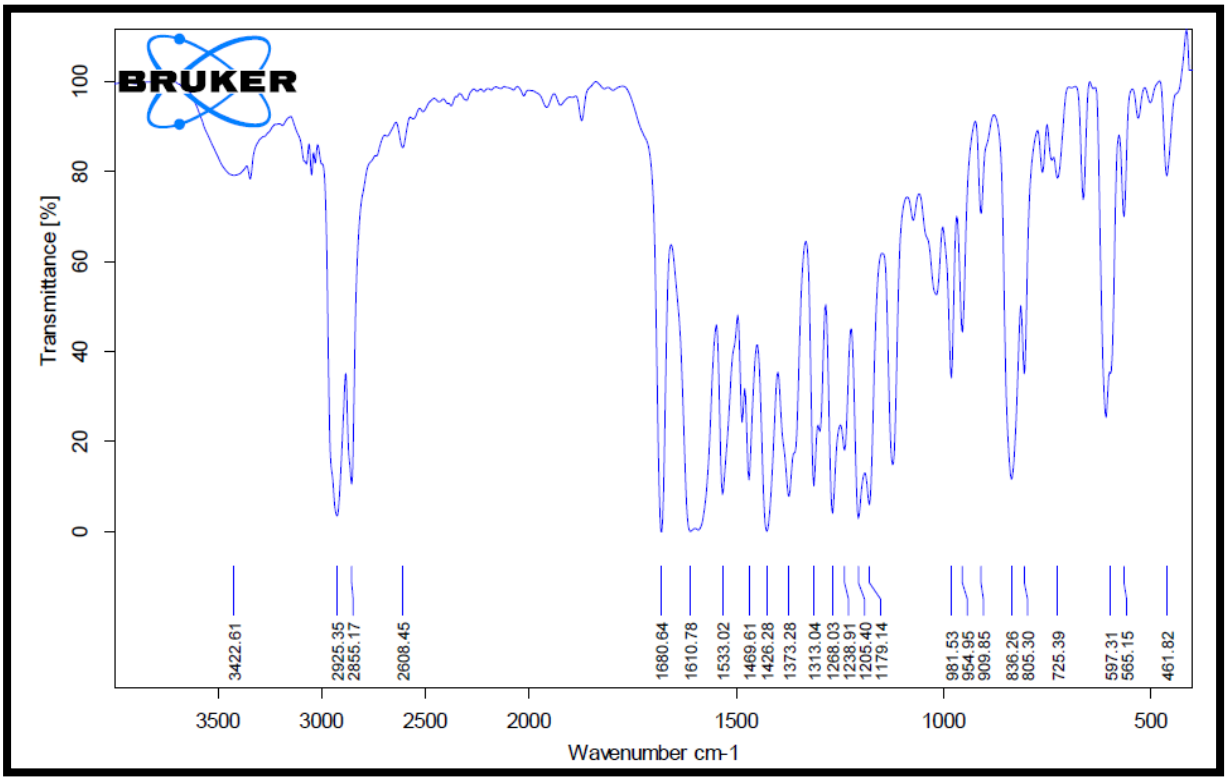

IR spectra of B8

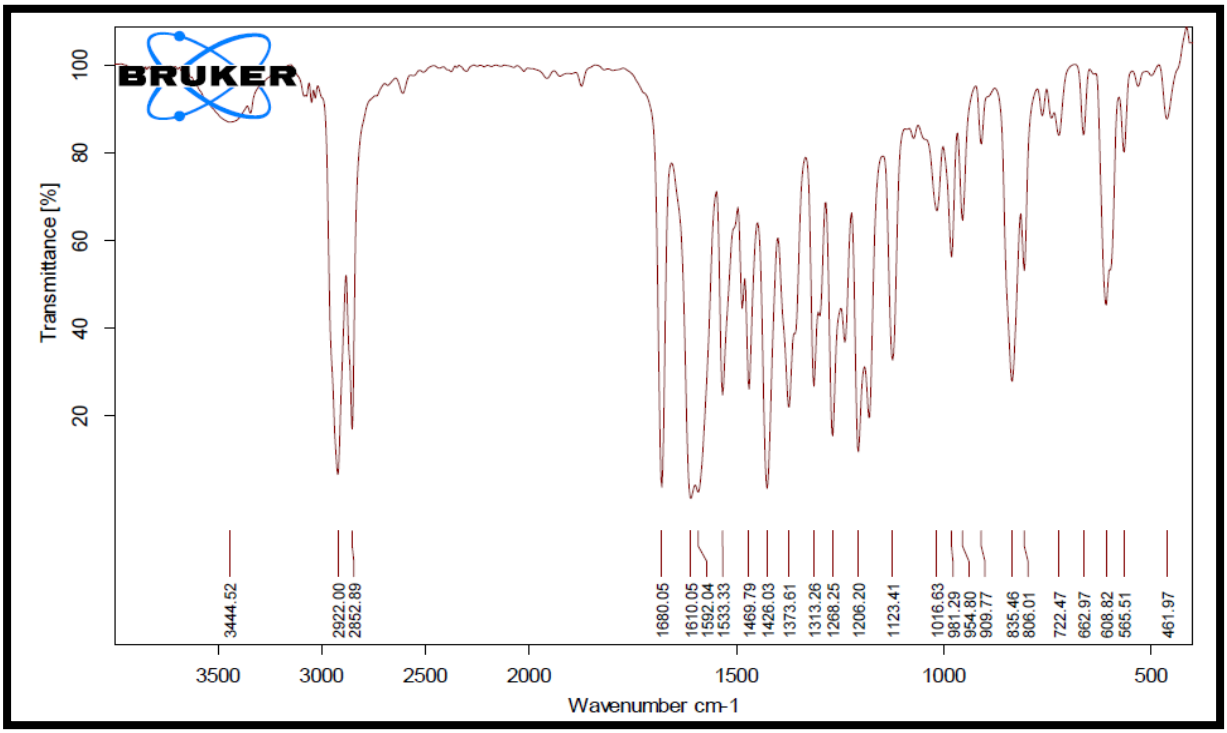

IR spectra of B10

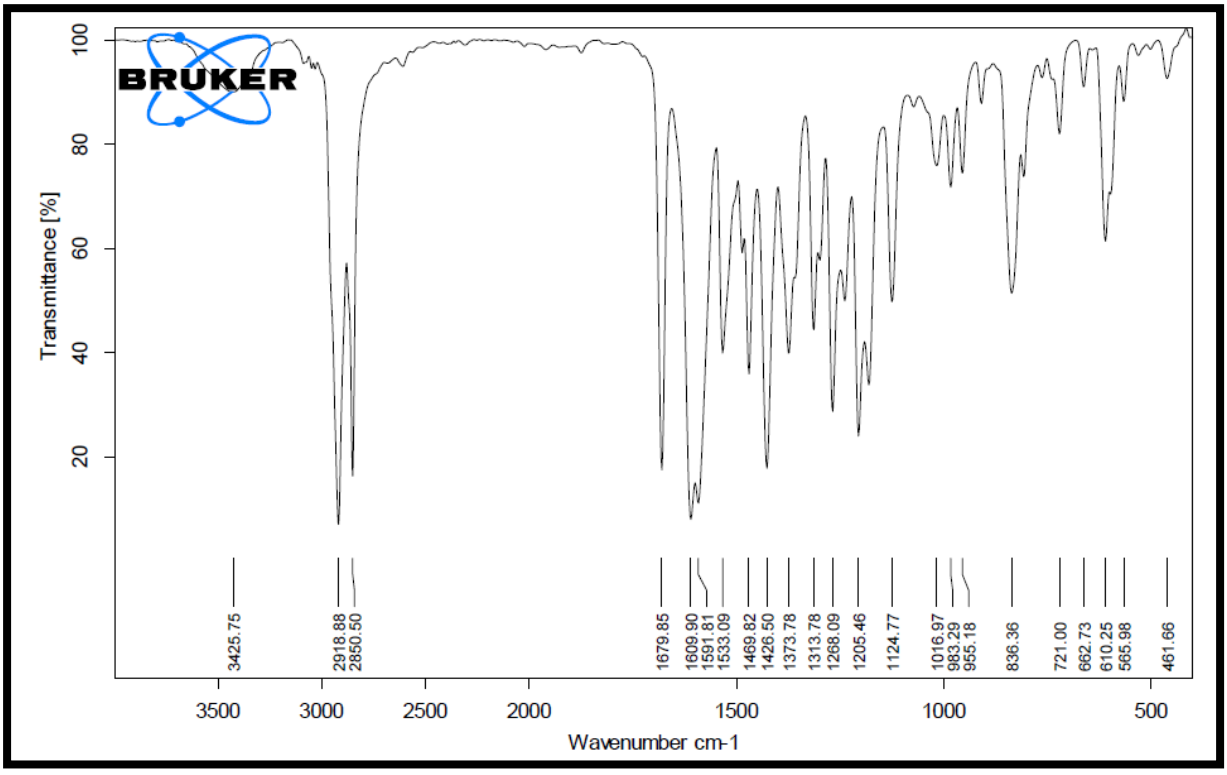

IR spectra of B16

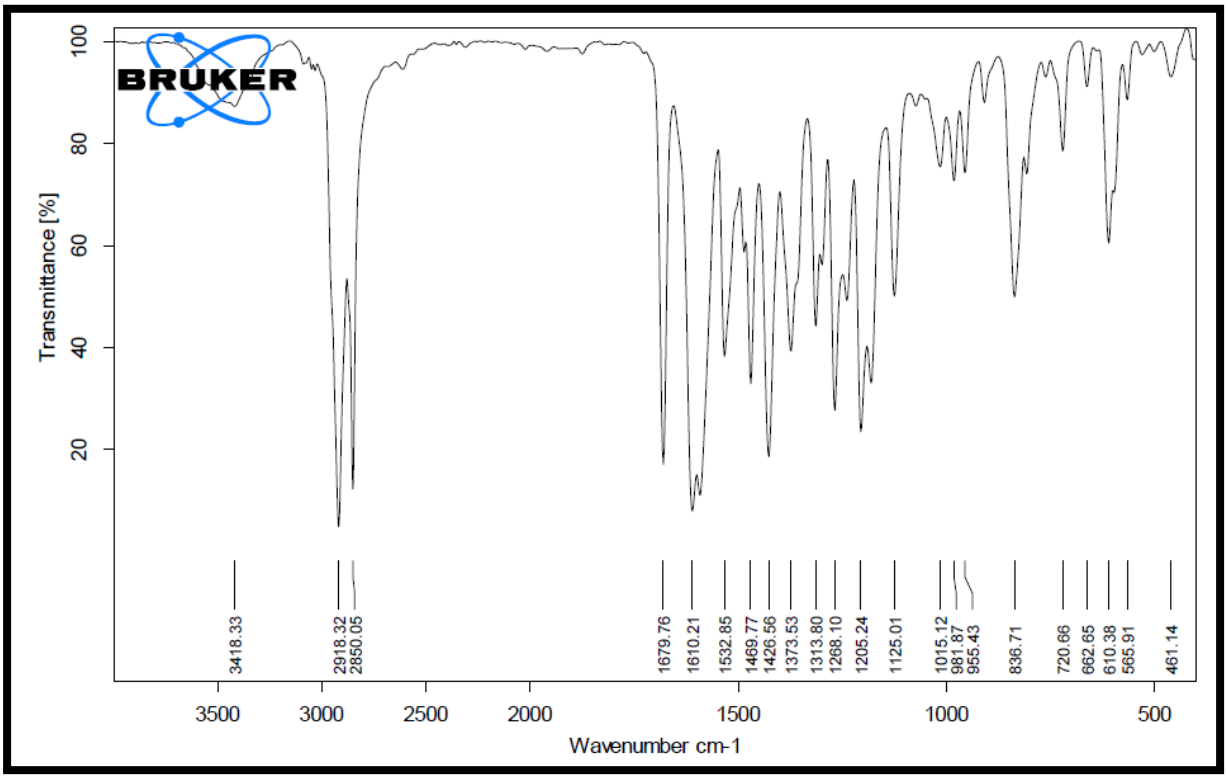

IR spectra of B18